Distributed Space-Time Block Coding in Wireless Cooperative Communications

CHENG Ho Ting

A Thesis Submitted in Partial Fulfilment
of the Requirements for the Degree of
Master of Philosophy
in
Information Engineering

August 2005

Abstract of thesis entitled:

Distributed Space-Time Block Coding in Wireless Cooperative Communications

Submitted by CHENG Ho Ting

for the degree of Master of Philosophy

at The Chinese University of Hong Kong in August 2005

In this thesis, we are going to study user cooperative communications or simply cooperative communications in wireless systems with the help of distributed space-time block coding. Through investigating carefully the case of 3-node system model (source, relay and destination), we first study its performance in terms of the bit-error-rate (BER) by deriving closed-form expressions for a distributed space-time block coded system, considering both perfect and imperfect channel estimation. We employ Alamouti's code [2] in a distributed fashion and show that with appropriate power control, the maximum diversity order is obtained. Our analysis also demonstrates the existence of an error floor due to channel estimation errors. For power imbalance, our analytical expressions provide tight bounds to simulation results. For balanced links, the lowest error floor and the optimal performance for imperfect channel estimation are obtained.

In addition, we further study its performance of distributed space-time block coding over time-varying channels. Following Jakes' time-varying channel model [17], we compare different reception schemes including maximum likelihood in [29], Alamouti's receiver, zero-forcing, decision-feedback and our newly considered detection called cooperative maximum likelihood. To analyze their BER performances,

we first employ the technique of pilot symbol assisted modulation (PSAM) to estimate the time-varying channel coefficients. Our simulation results show that cooperative maximum likelihood detection always has a privilege to achieve the best performance due to the diversity gain with the help of separated signal transmissions while the other detection methods achieve relatively worse but nearly the same BER performance. Second, under the ideal situations that the exact channel coefficients are available at the receiver, we derive closed-form expressions of reception methods of zero-forcing and decision-feedback. Our results show that by simulations and analytical expressions, the cooperative maximum likelihood detection and maximum likelihood detection in [29] outperform the others and the performance of the decision-feedback receiver is slightly better than that of the zero-forcing receiver. The worst one is Alamouti's receiver. In accordance with our numerical results, we find that as long as we can obtain the better channel estimates, we should first choose the cooperative maximum likelihood detector and maximum likelihood detector in [29], then the decision-feedback receiver, the zero-forcing receiver and Alamouti's receiver at last. On the whole, the effect of time-varying channels induces an error floor.

摘要

在這份論文中，我們利用分佈空間及時間塊編碼，研究無線系統的用戶合作通信或簡稱為合作通信。透過深入調查三結系統模式(來源、中轉和目的地)的情況，從而了解它的誤碼率(BER)表現，並就完善和不完善的通訊通道評估，推導出一個分佈空間及時間塊編碼系統的封閉表達式。我們使用分佈的 Alamouti 的編碼[2]，以適當的電能控制，顯示出我們能獲得最大分集次序。由於估計通訊通道的錯誤，我們的分析並且展示出錯誤地板的存在。在電能不平衡的狀態，我們的分析表達式對模仿結果提供緊密的區域。在平衡的鏈接，我們在不完善的通訊通道估計中可以獲得最低的錯誤地板和最好的表現。

另外，我們進一步研究時間變化的通訊通道對分佈空間及時間塊編碼的表現。從 Jakes 的時間變化通訊通道模型[17]，我們提出不同的接收器包括在[29]的最大概似法、Alamouti 的接收器、零強迫、決定反饋和我們的最近提出的探測器叫合作最大概似法。在分析它們 BER 的表現時，我們首先使用試驗標誌協助的模塊化技術(PSAM)來估計時間變化的通訊通道系數。我們的模仿結果顯示，由於分散傳送而獲得分集增益，合作最大概似法經常達到最佳的表現。其他接收方法的表現較差但獲得同樣 BER 的表現。其次，在理想的情況之下，即在接收器可以得到確切的通訊通道系數，我們推導出零強迫和決定反饋接收方法封閉表達式。由模仿結果和分析結果，我們得知合作最大概似法和[29]的最大概似法接收器表現比其他接收器較佳，決定反饋接收器的表現比零強迫的接收器好。最差的是 Alamouti 的接收器。根據分析的結果，我們發現只要能獲得更好的通訊通道估計，我們應該首先選擇合作最大概似法接收器和[29]的最大概似法接收器，然後決定反饋接收器和零強迫的接收器，而最後是 Alamouti 的接收器。總體上，時間變化通訊通道引致錯誤地板。

Acknowledgement

I would like to thank my supervisor, Prof. Tat-Ming LOK for his inquisitiveness, advices and support. He has helped me reach several milestones and given me tremendous encouragement. His insights always guided me to a right research direction. More importantly, I have gained a lot from his optimistic attitude. Let me express my sincere gratitude to Prof. LOK again.

I would also want to thank Prof. Murat UYSAL for many useful interactions and his supervision during my exchange program. Thanks also go to Hakam for his help and research ideas.

As always, I thank my family for inspiring me to pursue an academic career. Without them, I think I cannot complete my master degree.

Last, my most tender thanks go to my lover, Chi Yan. I would like to thank her by heart for accompanying me in my hardship. Her love is the best support in my life.

This work is dedicated to my family and Chi Yan.

Contents

List of Figures

List of Tables

Chapter 1

Introduction

1.1 Overview of Wireless Cooperative Communications

There is an increasing demand for wireless multimedia and interactive internet services, which require much higher speed data transmission and better power efficiency compared to current wireless communication systems. In wireless systems, however, fading will degrade the performance, which can be alleviated by different forms of diversity [17]. In particular, spatial diversity offers significant improvement in link reliability and spectral efficiency through the use of multiple antennas at the transmitter and/or receiver side [2, 8, 26, 27]. Although co-located multiple-antenna techniques are quite attractive for deployment in the cellular applications at base stations and have been already included in the 3G wireless standards, employing a large antenna array might not be practical at the cellular mobile devices as well as at nodes in ad-hoc mobile networks, due to the size and power limitation of the mobile terminals.

In a single-user scenario, cooperation is not possible. Yet, nearly all wireless systems operate in a multiuser fashion. Thus, the idea of user cooperative communications was born [14], where mobiles share their antennas to form a virtual

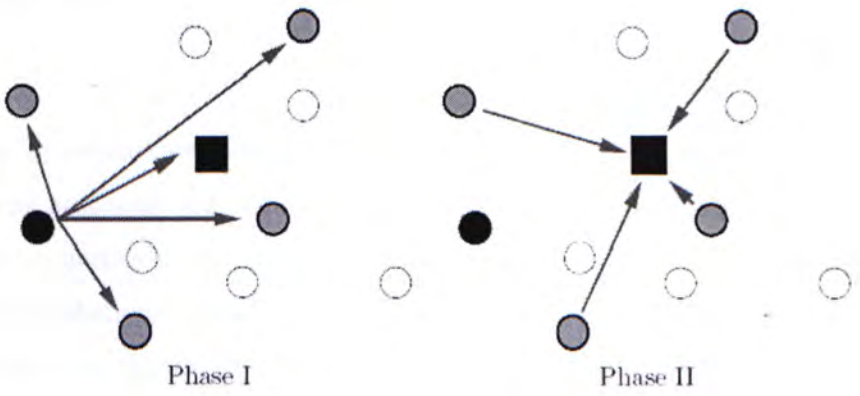

Figure 1.1: Illustration of a cooperative diversity scheme. First, the source (black circle) broadcasts the information to the destination (black square) as well as potential relays. The "partners" are shaded. Second, the cooperative nodes help transmit the information to the destination.

antenna array as if each terminal had as many transmit antennas as the virtual antenna array of cooperative terminals to simulate transmit diversity. This new form of spatial diversity is called user cooperative diversity or simply cooperative diversity.

1.2 Motivation

Consider a motivating example in Fig. 1.1 [13]: The source (black circle) transmits the information to the destination (black square). If their communication channel is subject to a deep fading, without cooperation, they cannot communicate reliably. In contrast, with appropriate cooperation, the source makes use of the surrounding nodes as partners which help transmit the information to the destination with some sort of transmission protocols. In this case, cooperative diversity can be achieved, thereby allowing more reliable and effective communications. And, we see that for

the same total transmit power, even though we increase the transmit power, we only get a coding gain in a non-cooperative case, but a diversity gain in a cooperative manner.

As far as we can see, user cooperation has the potential to be successfully used in wireless networks, e.g. ad hoc networks. The wireless ad hoc networks do not have a fixed network topology and infrastructure. Also, there are no central servers such as base stations. Simply, the mobile nodes or users communicate by forming a cluster based on mobile locations and channel conditions. If one node tries to send data to another node, this may involve several mobile-to-mobile communications as the direct link-to-link communication may not be possible. Then, cooperative communications play a prominent role here in providing dependability in communication channels and robustness to channel variations.

Most of the current related work, however, assumes that perfect knowledge of the channel fading coefficients is available at the receiver side of destination terminals [14, 15]. In practice, these channel coefficients must be estimated and then used in the detection process. In [4], we have studied the effect of imperfect channel estimation for distributed space-time block coding. Another practical issue is the time-varying channel. In reality, the channels are not static, but time-varying, which causes performance degradation and complexity of the receiver design. In this chapter, we will give an overview of the aforementioned issues namely,

- Distributed Space-Time Block Coding
- Imperfect Channel Estimation
- Time-Varying Channels

1.3 Distributed Space-Time Block Coding

Among many proposed cooperative schemes, distributed space-time block codes (DSTBC) are of great interest as the STBC discussed in [26] can be readily used in a distributed fashion for wireless communication networks if synchronization is possible. In particular, orthogonal STBC has been suggested for practical implementation due to its low decoding complexity at receiver. In chapter 3, we will introduce the DSTBC for the relay-assisted communication system proposed in [15] with performance analysis.

1.4 Imperfect Channel Estimation

In chapter 3, our work is based on the assumption that the perfect knowledge of channel fading coefficients is available at the receiver side for the destination terminal. In reality, channel fading coefficients must be estimated. In chapter 4, we will further investigate the BER performance for the DSTBC with estimated channel state information (CSI), providing analytical closed-form expressions. The content of chapter 4 is mainly from [4].

1.5 Time-Varying Channels

To extend the discussions of chapter 4, we focus on how time-varying channels alter the performance. In chapter 5, we analyze different reception schemes, namely cooperative maximum likelihood receiver, maximum likelihood receiver in [29], Alamouti's receiver, zero-forcing receiver, decision-feedback receiver, and compare their performances. First, we employ the pilot symbol assisted modulation (PSAM) to estimate the time-varying channel coefficients for assessing their BER. Second, under the assumption of ideal situations that the exact channel coefficients are available at the receiver, we derive closed-form expressions and discuss the discrepancies among the receivers.

1.6 Outline of the thesis

The thesis continues as follows: Chapter 2 is the background study. Then, we discuss the distributed space-time block coding in chapter 3. In chapter 4 and 5, we consider two practical topics that are imperfect channel estimation and time-varying channels respectively. We will draw a conclusion and prospect our future work in Chapter 6.

□ **End of chapter.**

Chapter 2

Background Study

In modern wireless world, people demand for services with high data rate transmission and low probability of error. They also request for good power efficiency to run certain applications in wireless environment. In order to meet the requirements, next-generation (third generation and beyond) wireless systems must exploit advanced transmission algorithms and techniques to guarantee the quality-of-service (QoS) desired by different applications. Thus far, the techniques currently being investigated and used for achieving the goals encompass signal processing, modulation, detection and various forms of diversity. Among them, diversity is of great importance because it is an effective way to maintain reliable communications.

In wireless networks, signal fading arising from multi-path propagation is a big issue, which means that mobile users or mobile nodes cannot communicate with the others and the destinations reliably. Nonetheless, diversity is an effective way to mitigate the effects of fading. By transmitting (partially) redundant copies of signals over essentially independent channel realizations, we can combat and average the channel variations with suitable receiver combining. Some classical forms of diversity are temporal diversity, frequency diversity and spatial diversity [17]:

- Temporal Diversity - Use different time slots separated by an interval longer

than the coherence time of the channel.

- Frequency Diversity - Use different frequency carriers separated by a distance larger than the coherence bandwidth of the channel.
- Spatial Diversity - Use multiple antennas separated wide enough with respect to the carrier wavelength.

In particular, exploiting spatial diversity is of great interest in the use of multi-antenna physical arrays at the transmitters and/or receivers in a wireless system.

Physical arrays offer space diversity to combat fading, or when sufficient knowledge of the channel conditions are available at both the transmitter and receiver, offer beamforming to combat both fading and interference from other terminals, and other wireless systems in the same band. As a result, physical arrays increase capacity and improve robustness to fading, thereby offering significant improvement in link reliability. Motivated by these possible gains, a great deal of research effort has focused on studying spatial diversity, including receive diversity and transmit diversity. In uplink, receive diversity is easily achieved as we can employ a large antenna array at the base station or the central server. In contrast, receive diversity is difficult to implement in downlink as it is not suitable due to size and power limitation at the mobile nodes. Thus, transmit diversity emerges. Yet, to extract diversity from multiple antennas at the transmitter, pre-processing or pre-coding prior to transmission is required. Let see the following example:

Example: Assume the same signal is transmitted from two different antennas without any pre-processing. Then, the received signal is given by

$$r = \sqrt{\frac{E_s}{2}} h_1 s + \sqrt{\frac{E_s}{2}} h_2 s + n \tag{2.1}$$

where E_s is the total transmit power, h_1 and h_2 are complex Gaussian random variables with zero mean and unit variance, i.e. $E[h_1] = E[h_2] = 0$, $E[|h_1|^2] =$

$E[|h_2|^2] = 1$, s is the transmitted signal and n is the noise. Now, (2.1) can be written as

$$r = \sqrt{E_s}\left(\frac{h_1}{\sqrt{2}} + \frac{h_2}{\sqrt{2}}\right)s + n \tag{2.2}$$

By defining $h = \frac{h_1}{\sqrt{2}} + \frac{h_2}{\sqrt{2}}$, we have

$$r = \sqrt{E_s}hs + n \tag{2.3}$$

where $E[|h|^2] = 1$. Now, we obtain an equivalent Single-Input-Single-Output (SISO) model. No diversity is provided. Thus, we notice that code designs are essential to make transmit diversity possible. In 1998, Alamouti proposed a simple space-time block code achieving full diversity [2]. The code matrix is shown below:

$$\mathcal{C} = \begin{bmatrix} x_1 & x_2 \\ -x_2^* & x_1^* \end{bmatrix}. \tag{2.4}$$

Alamouti's code is the first open-loop transmit diversity technique which provides full diversity with linear processing at the receiver complexity. Under the assumption that fading coefficients are constant over two symbol periods, the received signals for two consecutive time intervals are given

$$r_1 = h_1x_1 + h_2x_2 + n_1, \tag{2.5}$$

$$r_2 = h_1(-x_2^*) + h_2x_1^* + n_2, \tag{2.6}$$

If perfect channel state information (CSI) is available at the receiver, by using the maximum likelihood receiver, the best pair of signals $\hat{x}_1, \hat{x}_2$ is chosen, which minimizes the following distance metric

$$\begin{aligned} &d^2(r_1, h_1\hat{x}_1 + h_2\hat{x}_2) + d^2(r_2, -h_1\hat{x}_2^* + h_2\hat{x}_1^*) \\ &= |r_1 - (h_1\hat{x}_1 + h_2\hat{x}_2)|^2 + |r_2 - (-h_1\hat{x}_2^* + h_2\hat{x}_1^*)|^2 \end{aligned} \tag{2.7}$$

over all possible values of $(\hat{x}_1, \hat{x}_2)$. Expanding the above expression,

$$\begin{aligned} (\hat{x}_1, \hat{x}_2) = \arg \min_{(\hat{x}_1,\hat{x}_2)\in S^2} \{&\left(|h_1|^2 + |h_2|^2 - 1\right)|\hat{x}_1|^2 + d^2(\tilde{x}_1, \hat{x}_1) \\ &+ \left(|h_1|^2 + |h_2|^2 - 1\right)|\hat{x_2}|^2 + d^2(\tilde{x}_2, \hat{x}_2)\} \end{aligned} \tag{2.8}$$

where S^2 is the set of all possible pairs and $\tilde{x}_1, \tilde{x}_2$ are decision statistics constructed by combining the received signals, i.e.

$$\tilde{x}_1 = h_1^* r_1 + h_2 r_2^* = \left(|h_1|^2 + |h_2|^2\right) x_1 + h_1^* n_1 + h_2 n_2^* \tag{2.9}$$

$$\tilde{x}_2 = h_2^* r_1 - h_1 r_2^* = \left(|h_1|^2 + |h_2|^2\right) x_2 - h_1 n_2^* + h_2^* n_1. \tag{2.10}$$

Because Alamouti's code is orthogonal, it means that the decoding rule can be decomposed into two separate parts:

$$\hat{x}_1 = \arg\min_{\hat{x}_1 \in S} \left(|h_1|^2 + |h_2|^2 - 1\right) |\hat{x}_1|^2 + d^2\left(\tilde{x}_1, \hat{x}_1\right) \tag{2.11}$$

$$\hat{x}_2 = \arg\min_{\hat{x}_2 \in S} \left(|h_1|^2 + |h_2|^2 - 1\right) |\hat{x}_2|^2 + d^2\left(\tilde{x}_2, \hat{x}_2\right). \tag{2.12}$$

For M-PSK, $|x|^2$ is a constant and so

$$\hat{x}_1 = \arg\min_{\hat{x}_1 \in S} d^2\left(\tilde{x}_1, \hat{x}_1\right) \tag{2.13}$$

$$\hat{x}_2 = \arg\min_{\hat{x}_2 \in S} d^2\left(\tilde{x}_2, \hat{x}_2\right), \tag{2.14}$$

which speeds up the decoding process.

Alamouti's scheme was merely proposed for 2 transmit antennas. The concept was generalized for more transmit antennas by Tarokh et al. who have investigated and discussed different facets of space-time block codes (STBC). They proposed the design criteria for good space-time codes. One important aspect is the diversity order determining the slope of the curve of error probability against signal-to-noise ratio. In order to achieve maximum diversity order, the code matrix has to be full rank, which is called the rank criterion [27]. Based on Radon-Hurwitz Theorem [18], Tarokh showed that full-rate orthogonal STBC (OSTBC) exists for very restricted antenna and modulation configurations. Let R be rate and M be number of transmit antennas

- R=1, OSTBC for real constellations for any number of M
- R=1, OSTBC for complex constellations possible only for $M = 2$ (Alamouti's scheme)

- R=1/2, OSTBC always possible for any number M
- R=3/4, OSTBC for complex constellations $M = 3, 4$

The foregoing studies are about the conventional (orthogonal) space-time block coding.

Several studies [17] have shown that, aside from suitable encoding and decoding algorithms, the key to leveraging spatial diversity with physical arrays is to have separation among the antennas on the order of several wavelengths of the carrier frequency so that the fading coefficients are uncorrelated. As carrier frequencies increase, this constraint becomes less restrictive. However, terminal size also decreases with time and circuit integration, thereby limiting the number of antennas that can be effectively placed at a transmitter or receiver. Also, with the power limitations of mobile terminals, employing a large antenna array might not be practical at the cellular mobile devices as well as at nodes in ad-hoc mobile networks, which falls through the diversity gain at mobile stations. Thus, it seems that uplink transmit diversity is not feasible before the concept of user cooperation emerges.

Recently, the user cooperative diversity has been demonstrated to provide an effective way of improving spectral and power efficiency of the wireless networks without the additional complexity of multiple antennas [12, 14, 22, 23]. The basic idea behind cooperative diversity rests on the observation that in a wireless environment, the signal transmitted by the source nodes is overheard by other nodes, which can be defined as partners. The source and its partners can jointly process and transmit their information, creating a virtual antenna array although each of them is equipped with only one antenna. The chief philosophy is that as not all mobile nodes are active at the same time, a user can seek extra resources from the idle nodes. Also, there is no cost, in terms of transmit power, associated with transmitting to both the intended destinations and the nodes nearby, since the wireless

transmissions are omnidirectional. Thus, the user of interest and his partners act as a virtual antenna array, which simulates the transmitter diversity. With diversity gain, the error probability can be reduced tremendously and hence we can maintain reliable communications and meet QoS requirements. Through cooperation, instead of fighting for the limited resources, it is more effective and opportunistic to allocate these resources among all users with the help of distributed protocols and robust detection techniques.

In current literature, some work on cooperative diversity addresses information theoretical aspects of cooperative networks. In [22, 23], an information theoretic model is presented, for which achievable rate regions and outage probabilities are examined. In a CDMA implementation, two users cooperate by transmitting each bit over two successive intervals. This work is extended in [14] proposing an amplify-and-forward relay as the best option under most situations of interest. Another cooperative method called coded cooperation is suggested in [11], in which symbols are not repeated by the partner. Instead, the codeword of each user is partitioned into two sets: one partition is transmitted by the user, and the other by the partner. The authors show that coded cooperation provides significant performance gains for a variety of channel conditions. Recently, conventional orthogonal space-time block coding has been suggested for practical implementation of user cooperation in a distributed fashion [14]. In [15], the authors analyze distributed space-time block coding operating in amplify-and-forward (AF) mode through the derivation of pairwise error probability (PEP) expression. They show that the original design criteria for the STBC in [26] (i.e. rank and determinant criteria) still apply to the design of distributed STBC schemes with appropriate power control algorithms.

In fact, there are loads of research work on channel estimation for conventional space-time coded system [6, 10]. To estimate channel coefficients, one possible way

is to use pilot symbols [3]. In this pilot symbol assisted transmission, pilot symbols are inserted in the data stream. At the receiver, these symbols are extracted and some interpolation methods are used to construct fading estimates. Yet, these estimates are not usually accurate, thereby causing performance degradation. Some previous work studied the optimal performance of the channel estimator [3]. Some compared the bit-error-rate under channel estimation errors with that under perfect channel knowledge with the concept of "closeness" [6]. Some gave analytical expressions for performance analysis [10].

However, most of the work focuses insofar on the cooperative system models with perfect channel state information and time-invariant channels. In this thesis, we aim at investigating and analyzing these two facets of user cooperative communications, namely distributed space-time block coding with imperfect channel estimation and time-varying channels.

□ **End of chapter.**

Chapter 3

Distributed Space-Time Block Coding

3.1 Introduction

As we have discussed, there are many cooperative schemes suitable for wireless ad hoc networks. Among all, distributed space-time block codes (DSTBC) are of great interest as the conventional STBC can be readily used in a distributed fashion. In this chapter, we consider the case of single relay operating in the amplify-and-forward (AF) mode. We examine its bit-error-rate (BER) performance and the characteristics of this cooperation system model [4].

3.2 System Model

Consider the fading relay channel shown in Fig. 3.1. Data is to be transmitted from the source terminal S to the destination terminal D with the assistance of the relay terminal R. All terminals are equipped with single antenna. Notice that a terminal cannot transmit and receive simultaneously. The relay terminal assists in communication with the destination terminal by amplifying-and-forwarding (AF) the received signal. In the AF operation mode, the relay terminal simply amplifies

Time Slot	Protocol
1	S → R
2	S → D, R → D

Table 3.1: A TDMA-based protocol. S, R and D stand for the source, relay and the destination nodes respectively. $X \rightarrow Y$ denotes the link from terminal X to terminal Y.

and retransmits the signal received from the source terminal (the signal received at the relay terminal is corrupted by fading and additive noise). No demodulation or decoding of the received signal is performed in this case.

The cooperation protocol we adopt is shown in Table 3.1, which is proposed by [15]: S communicates with R during the first signaling interval and there is no transmission from S to D within this period. In the second signaling interval, both R and S communicate with D. For $R \rightarrow D$ link, an AF mode is used, in which R amplifies and forwards the signal received from S in the first signaling interval. Concerning this protocol, it can be justified that the destination node may be engaged in data transmission to another terminal in the first signaling interval. Therefore, the transmitted signal is received merely at the relay terminal which then amplifies and forwards the signal in the next interval.

Let the signals transmitted by the source terminal during the first and second time slots denoted as x_1 and x_2 respectively. We assume binary phase shift keying (BPSK) modulation with unit energy for symbols, i.e. $E[|x_i|^2] = 1$, for $i = 1, 2$. Thus, in the first signaling interval, the signal received at the relay terminal is given by

$$r_R = \sqrt{E_{SR}}\, h_{SR}\, x_1 + n_R \tag{3.1}$$

where E_{SR} stands for the average received energy at the relay terminal from the source terminal, considering the path loss and possible shadowing effects in $S \rightarrow R$

link. h_{SR} denotes the complex fading coefficient over $S \rightarrow R$ link and it is modeled as a zero-mean complex Gaussian random variable with unit variance, leading to a Rayleigh fading. n_R is a zero-mean complex Gaussian random variable with variance $N_0/2$ per dimension, which models the additive noise.

The relay terminal normalizes the received signal r_R by a factor of $\sqrt{E[|r_R|^2]}$ to ensure the unity of the average energy and re-transmits the signal in the second signaling interval. Therefore, the received signal at the destination terminal in the second time slot is given by

$$r = \sqrt{E_{SD}} h_{SD} x_2 + \sqrt{E_{RD}} h_{RD} \frac{r_R}{\sqrt{E[|r_R|^2]}} + \hat{n} \tag{3.2}$$

Likewise, E_{SD} and E_{RD} stand for the average received energy at the destination terminal, considering the path loss and possible shadowing effects in $S \rightarrow D$ link and $R \rightarrow D$ link respectively. h_{SD} and h_{RD} denote the complex fading coefficients over $S \rightarrow D$ link and $R \rightarrow D$ link respectively and they are modeled as zero-mean complex Gaussian random variables with unit variance, leading to a Rayleigh fading. $\hat{n}$ is a zero-mean complex Gaussian random variable with variance $N_0/2$ per dimension, which models the additive noise. Replacing (3.1) and the normalization factor $E[|r_R|^2] = E_{SR} + N_0$ in (3.2), we have

$$r = \sqrt{E_{SD}} h_{SD} x_2 + \sqrt{\frac{E_{SR} E_{RD}}{E_{SR} + N_0}} h_{RD} h_{SR} x_1 + \tilde{n} \tag{3.3}$$

where $\tilde{n} = \sqrt{\frac{E_{RD}}{E_{SR}+N_0}} h_{RD} n_R + n_D$, with zero mean and variance of $E[|\tilde{n}|^2] = N_0 \left(1 + \frac{E_{RD}}{E_{SR}+N_0}\right)$. Following [28], we can write the received signal as

$$r = \alpha h_1 x_1 + \beta h_2 x_2 + n \tag{3.4}$$

where $h_1 = h_{SR} h_{RD}$ and $h_2 = h_{SD}$. n is a zero-mean complex Gaussian random

variable with variance $N_0/2$ per dimension. Here, α and β are defined as

$$\alpha = \sqrt{\frac{E_{SR}/N_0}{1 + E_{SR}/N_0 + E_{RD}/N_0}}\sqrt{E_{RD}}, \tag{3.5}$$

$$\beta = \sqrt{\frac{1 + E_{SR}/N_0}{1 + E_{SR}/N_0 + E_{RD}/N_0}}\sqrt{E_{SD}} \tag{3.6}$$

respectively.

In [15], pairwise error probability (PEP) is analyzed, meaning that this relay-assisted or cooperative communication using a space-time code can achieve second order diversity, just like the case of co-located antennas. Thus, after setting up the above transmission model given by (3.4), in conjunction with (3.5) and (3.6), we now introduce space-time coding across the transmitted signals, i.e. x_1 and x_2. For the case of one relay terminal (as considered here), we use STBC designated for two transmit antennas, Alamouti's scheme, where the code matrix is defined as

$$\mathcal{C} = \begin{bmatrix} x_1 & x_2 \\ -x_2^* & x_1^* \end{bmatrix}. \tag{3.7}$$

The received signals are now given as

$$r_1 = \alpha h_1 x_1 + \beta h_2 x_2 + n_1, \tag{3.8}$$

$$r_2 = -\alpha h_1 x_2^* + \beta h_2 x_1^* + n_2. \tag{3.9}$$

3.3 BER Analysis by Characteristic Equations

We consider the BER expressions using characteristic equations. In this section, we fix h_{RD} and convert the received signals into a matrix form:

$$\begin{bmatrix} r_1 \\ -r_2^* \end{bmatrix} = \begin{bmatrix} \alpha h_1 & \beta h_2 \\ -\beta h_2^* & \alpha h_1^* \end{bmatrix} \begin{bmatrix} x_1 \\ x_2 \end{bmatrix} + \begin{bmatrix} n_1 \\ -n_2^* \end{bmatrix} \tag{3.10}$$

or

$$\mathbf{r} = \mathbf{H}\mathbf{x} + \mathbf{n}. \tag{3.11}$$

Let $\boldsymbol{\Upsilon} = [\Upsilon_1 \ \Upsilon_2]^T = \mathbf{H}^*\mathbf{r}$ and due to symmetry, we can only consider

$$\begin{aligned}
\Upsilon_1 &= \alpha h_1^* r_1 + \beta h_2 r_2^* && (3.12)\\
&= \alpha h_1^* \left(\alpha h_1 x_1 + \beta h_2 x_2 + n_1\right) + \beta h_2 \left(-\alpha h_1 x_2^* + \beta h_2 x_1^* + n_2\right)^* && (3.13)\\
&= \alpha h_1^* \left(\alpha h_1 x_1 + n_1\right) + \beta h_2 \left(\beta h_2^* x_1 + n_2^*\right) && (3.14)\\
&= \sum_{k=1}^{2} Re\left\{X_k Y_k^*\right\} && (3.15)
\end{aligned}$$

where

$$X_1 = \alpha h_1^* = \sqrt{\frac{E_{SR}/N_0}{1 + E_{SR}/N_0 + E_{RD}/N_0}}\sqrt{E_{RD}}h_1^*, \tag{3.16}$$

$$X_2 = \beta h_2 = \sqrt{\frac{1 + E_{SR}/N_0}{1 + E_{SR}/N_0 + E_{RD}/N_0}}\sqrt{E_{SD}}h_2, \tag{3.17}$$

$$Y_1 = \left(\alpha h_1 x_1 + n_1\right)^*, \tag{3.18}$$

$$Y_2 = \left(\beta h_2^* x_1 + n_2^*\right)^*. \tag{3.19}$$

And the decision variable at the detector can be expressed as a special case of the general quadratic form [17]:

$$D = \sum_{k=1}^{L} \left(A|X_k|^2 + B|Y_k|^2 + CX_k Y_k^* + C^* X_k^* Y_k\right). \tag{3.20}$$

Thus, in our case, $L = 2, A = B = 0$ and $C = C^* = 1/2$. The error event occurs when $D < 0$. Then we start deriving the BER from the characteristic function of d_k, where

$$d_k = A|X_k|^2 + B|Y_k|^2 + CX_k Y_k^* + C^* X_k^* Y_k, \tag{3.21}$$

and its characteristic function is

$$\psi_{d_k}(j\upsilon) = \frac{\upsilon_{1k}\upsilon_{2k}}{\left(\upsilon + j\upsilon_{1k}\right)\left(\upsilon - j\upsilon_{2k}\right)} \exp\left[\frac{\upsilon_{1k}\upsilon_{2k}\left(-\upsilon^2\lambda_{1k} + j\upsilon\lambda_{2k}\right)}{\left(\upsilon + j\upsilon_{1k}\right)\left(\upsilon - j\upsilon_{2k}\right)}\right] \tag{3.22}$$

where the parameters $\upsilon_{1k}, \upsilon_{2k}, \lambda_{1k}$ and λ_{2k} depend on the means $\bar{X}_k$ and $\bar{Y}_k$ and the second (central) moments $\mu_{x_k x_k}$, $\mu_{y_k y_k}$ and $\mu_{x_k y_k}$ of the complex Gaussian variables X_k and Y_k. Given $|h_{RD}|$, the probability of error is given by (See Appendix A)

$$P(e) = \frac{-\upsilon_{11}\upsilon_{12}\upsilon_{22}}{(\upsilon_{21}+\upsilon_{11})(\upsilon_{21}+\upsilon_{12})(\upsilon_{21}-\upsilon_{22})} + \frac{-\upsilon_{11}\upsilon_{12}\upsilon_{21}}{(\upsilon_{22}+\upsilon_{21})(\upsilon_{22}-\upsilon_{21})(\upsilon_{22}+\upsilon_{12})} \tag{3.23}$$

where

$$\upsilon_{11} = \sqrt{\frac{4}{N_0^2} + \frac{1}{\frac{1}{4}\left(\frac{E_{SR}E_{RD}}{1+E_{SR}/N_0+E_{RD}/N_0}\right)|h_{RD}|^2}} - \frac{2}{N_0} \tag{3.24}$$

$$\upsilon_{12} = \sqrt{\frac{4}{N_0^2} + \frac{1}{\frac{1}{4}\left(\frac{E_{SR}E_{RD}}{1+E_{SR}/N_0+E_{RD}/N_0}\right)|h_{RD}|^2}} + \frac{2}{N_0} \tag{3.25}$$

$$\upsilon_{21} = \sqrt{\frac{4}{N_0^2} + \frac{1}{\frac{1}{4}\left(\frac{(E_{SR}+N_0)E_{SD}}{1+E_{SR}/N_0+E_{RD}/N_0}\right)}} - \frac{2}{N_0} \tag{3.26}$$

$$\upsilon_{22} = \sqrt{\frac{4}{N_0^2} + \frac{1}{\frac{1}{4}\left(\frac{(E_{SR}+N_0)E_{SD}}{1+E_{SR}/N_0+E_{RD}/N_0}\right)}} + \frac{2}{N_0}. \tag{3.27}$$

Though we can obtain the closed-form expression for BER by characteristic equations, the expression (3.23) does not give any explicit insight how different system parameters affect the probability of error. In order to have a better closed-form expression, we analyze its BER again by introducing the error terms.

3.4 BER Analysis by Error Terms

In this section, by introducing the error terms defined in Appendix B, we derive the closed-form BER expressions under perfect channel estimation and time-invariant channels. Here, we consider both non-fading and fading $R \rightarrow D$ links.

3.4.1 Non-fading $R \rightarrow D$ link

We start by considering that the $R \rightarrow D$ link is static (i.e. $h_{RD} = 1$). Define the average signal-to-noise ratio, $\bar{\gamma}_i$ where $i = 1, 2$, as

$$\bar{\gamma}_1 = \frac{E[\alpha^2|h_1|^2]}{N_0} = \frac{E_{SR}/N_0 \cdot E_{RD}/N_0}{1 + E_{SR}/N_0 + E_{RD}/N_0} \cdot |h_{RD}|^2, \tag{3.28}$$

$$\bar{\gamma}_2 = \frac{E[\beta^2|h_2|^2]}{N_0} = \frac{(1 + E_{SR}/N_0) \cdot E_{SD}/N_0}{1 + E_{SR}/N_0 + E_{RD}/N_0} \tag{3.29}$$

for $S \rightarrow R \rightarrow D$ and $S \rightarrow D$ links respectively. The exact closed-form BER expression is given by (See Appendix B)

$$P(e) = \frac{1}{2}\left(1 + \frac{\bar{\gamma}_1}{\bar{\gamma}_2 - \bar{\gamma}_1}\sqrt{\frac{\bar{\gamma}_1}{1 + \bar{\gamma}_1}} + \frac{\bar{\gamma}_2}{\bar{\gamma}_1 - \bar{\gamma}_2}\sqrt{\frac{\bar{\gamma}_2}{1 + \bar{\gamma}_2}}\right) \tag{3.30}$$

for $\bar{\gamma}_1 \neq \bar{\gamma}_2$.

When an appropriate power control is employed, i.e. $E_{SD} = E_{RD}$, and if $E_{SR}/N_0 \gg 1$, then $\bar{\gamma}_1 = \bar{\gamma}_2 = \bar{\gamma}$,

$$\bar{\gamma} = \frac{E_{SR}/N_0 \cdot E_{SD}/N_0}{1 + E_{SR}/N_0 + E_{RD}/N_0}. \tag{3.31}$$

In this case, BER expression is given by (See Appendix B)

$$P(e) = \frac{1}{2}\left(1 - \frac{3 + 2\bar{\gamma}}{2 + 2\bar{\gamma}}\sqrt{\frac{\bar{\gamma}}{1 + \bar{\gamma}}}\right). \tag{3.32}$$

3.4.2 Fading $R \rightarrow D$ link

Now, we consider the case where the $R \rightarrow D$ link is subject to fading. For an exact BER expression, we need to perform an expectation over (3.30) with respect to $|h_{RD}|$ which follows a Rayleigh distribution. Unfortunately, this does not explicitly yield a closed-form BER expression. Yet, under a high SNR assumption, (3.30)

reduces to

$$P(e||h_{RD}|) \approx \frac{1}{4}\frac{1}{\bar{\gamma}_1\bar{\gamma}_2} \tag{3.33}$$

$$= \frac{1}{4}\frac{\left(1+\frac{E_{SR}}{N_0}+\frac{E_{RD}}{N_0}\right)^2}{\frac{E_{SR}}{N_0}\cdot\frac{E_{SD}}{N_0}\cdot\frac{E_{RD}}{N_0}\cdot\left(1+\frac{E_{SR}}{N_0}\right)\cdot|h_{RD}|^2} \tag{3.34}$$

yielding

$$P(e) \approx -\frac{1}{4}\frac{\left(1+\frac{E_{SR}}{N_0}+\frac{E_{RD}}{N_0}\right)^2}{\frac{E_{SR}}{N_0}\cdot\frac{E_{SD}}{N_0}\cdot\frac{E_{RD}}{N_0}\cdot\left(1+\frac{E_{SR}}{N_0}\right)}\lim_{z\to 0} Ei(z). \tag{3.35}$$

Here, $Ei(z)$ is an exponential integral function defined as $Ei(z) = -\int_{-z}^{\infty}\exp(-t)t^{-1}dt$ [9]. For small z (i.e. around the origin), $Ei(z)$ can be expanded as a truncated power series as

$$Ei(z) = C + ln(z) + z + \frac{z^2}{4} + \frac{z^3}{18} \tag{3.36}$$

where C is a Euler's constant [1].

3.5 Performance

3.5.1 Accuracy of Analytical Expressions

First, we compare our analytical BER expressions given by (3.30) and (3.35) with simulation results in [15]. We consider E_{SR}/N_0 = 10dB, 30dB and $E_{SD} = E_{RD}$. As illustrated in Fig. 3.2, simulation and analytical results match perfectly for the static $R \to D$ link while for the fading $R \to D$ link, our analytical BER expression serves as a tight bound to the simulated one due to high SNR assumption used in the derivation. We observe that there is a performance loss about 4dB due to the presence of fading in $R \to D$ link.

3.5.2 Observation of Second-order Diversity

With power control

For $E_{SD} = E_{RD}$, Fig. 3.3 illustrates our analytical BER expressions for a wider range of E_{SD}/N_0. For static and Rayleigh fading $R \to D$ links, we plot using (3.30) and (3.35) respectively. For reasonably high E_{SR}/N_0, e.g. 20dB and 30dB, the curves achieve second-order diversity. For low E_{SR}/N_0, e.g. 10dB, second-order diversity is not clearly observed as the source-to-relay channel is too noisy. Notice that there exists an error floor that appears in the high SNR region.

To locate the error floor, take $E_{SD} \to \infty$, then

$$\bar{\gamma}_1 \to \frac{E_{SR}}{N_0}, \tag{3.37}$$

$$\bar{\gamma}_2 \to 1 + \frac{E_{SR}}{N_0}. \tag{3.38}$$

Thus, the BER is lower bounded by

$$P_{LB}(e) = \frac{1}{2}\left(1 + \frac{E_{SR}}{N_0}\sqrt{\frac{E_{SR}/N_0}{1+E_{SR}/N_0}} - (1+\frac{E_{SR}}{N_0})\sqrt{\frac{1+E_{SR}/N_0}{2+E_{SR}/N_0}}\right). \tag{3.39}$$

In esssence, we do not know at which E_{SR}/N_0 value the error flooring effect becomes significant as the function is decreasing after the point of infection. Nonetheless, we know from inspection that the error floor appears roughly at the point when E_{SD}/N_0 slightly exceeds E_{SR}/N_0, giving us some information how to design the system and eschew the error floor.

Without power control

We then concern that no power control is implemented. For the sake of simplification, let $E_{SD} = nE_{RD}$, where n is a positive number. Again, we plot the curves using (3.30) and (3.35) for $n = 100,\ 10,\ 1,\ 0.1,\ 0.01$ and $E_{SR}/N_0 = 30\text{dB},\ 10\text{dB}$. In Fig. 3.4, with $E_{SR}/N_0 = 30\text{dB}$ for static $R \to D$ link, all curves achieve second-order diversity, but in different regions. When $E_{SD} \leq E_{RD}$, the curves realize second-order

diversity in the lower SNR region but have a higher error floor. On the contrary, when $E_{SD} > E_{RD}$, the curves achieve second-order diversity in the relatively higher SNR region and obtain a lower error floor. In case of Rayleigh fading, with performance loss incurred, all curves, except the last one, achieve second-order diversity shown in Fig. 3.5, like the static case. Yet, with $E_{SR}/N_0 = 10$dB, for static $R \to D$ link shown in Fig. 3.6, there are only three curves (out of five) with $E_{SD} \geq E_{RD}$, which can achieve second-order diversity in the low SNR region, unlike the previous cases. Consider the Rayleigh fading in Fig. 3.7, only two curves with $E_{SD} > E_{RD}$ can achieve second-order diversity. On the whole, the curves with higher E_{SR}/N_0 values are able to realize second order diversity and obtain the lower error probability in the high SNR region.

From the analytical point of view, under the power imbalance, (3.35) reduces to

$$P(e) \propto \frac{1}{n} \tag{3.40}$$

which agrees with the graphs. Thus, with this relation, it further gives us some insights to design the system operating in the effective region.

3.6 Summary

In this chapter, we have presented the distributed space-time block coding used in the relay-assisted communication system. We have derived closed-form BER expressions under perfect channel estimation and time-invariant channels. We have also considered the performance of the system. Our results indicate that maximum diversity order is achieved with an appropriate power control and a reasonable E_{SR}/N_0 value. Besides, we have discussed the appearance of the error floor and how to eschew this by careful selection of SNR ranges, thereby facilitating effective and reliable communications in cooperative networks.

□ **End of chapter.**

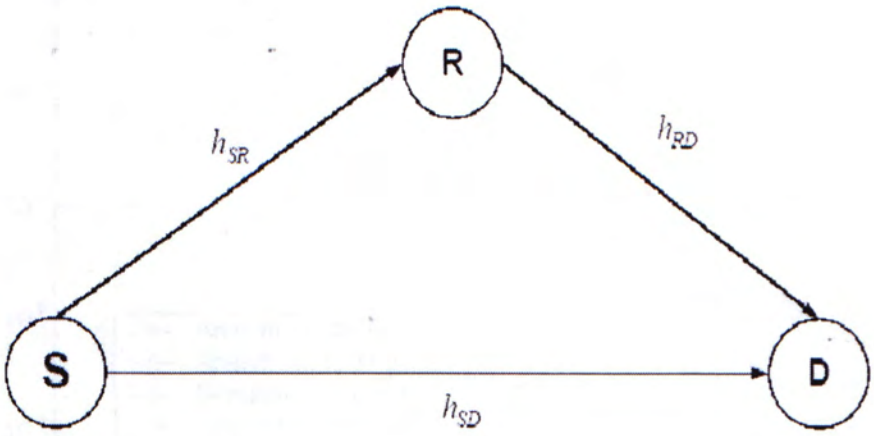

Figure 3.1: Schematic representation of relay-assisted transmission.

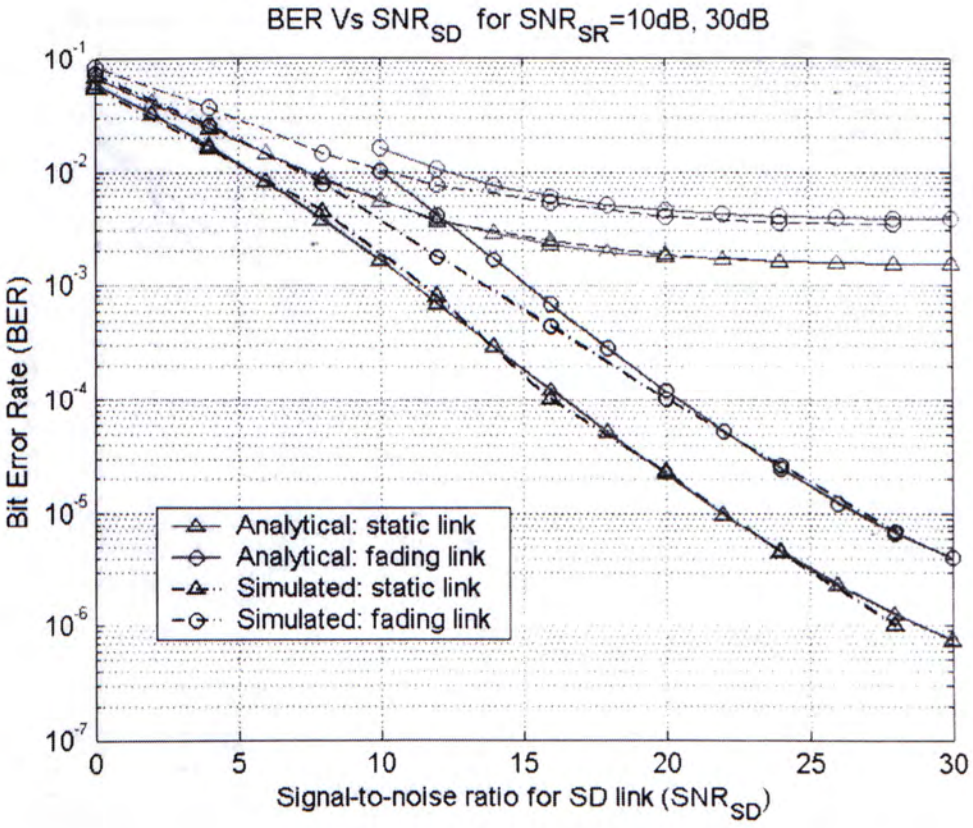

Figure 3.2: Comparison of simulation results in [15] and our analytical results. Thin curves: $E_{SR}/N_0 = 10$dB; Thick curves: $E_{SR}/N_0 = 30$dB.

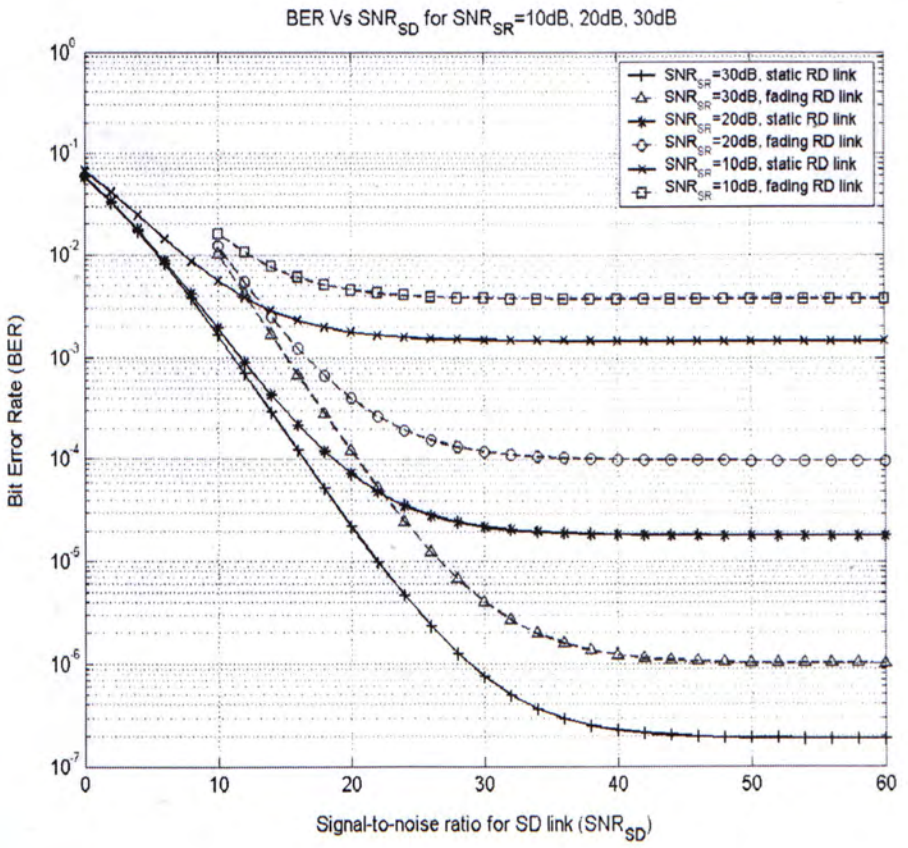

Figure 3.3: BER for static and fading $R \rightarrow D$ links under different E_{SR}/N_0 values, i.e. $E_{SR}/N_0 =$ 10dB, 20dB, 30dB.

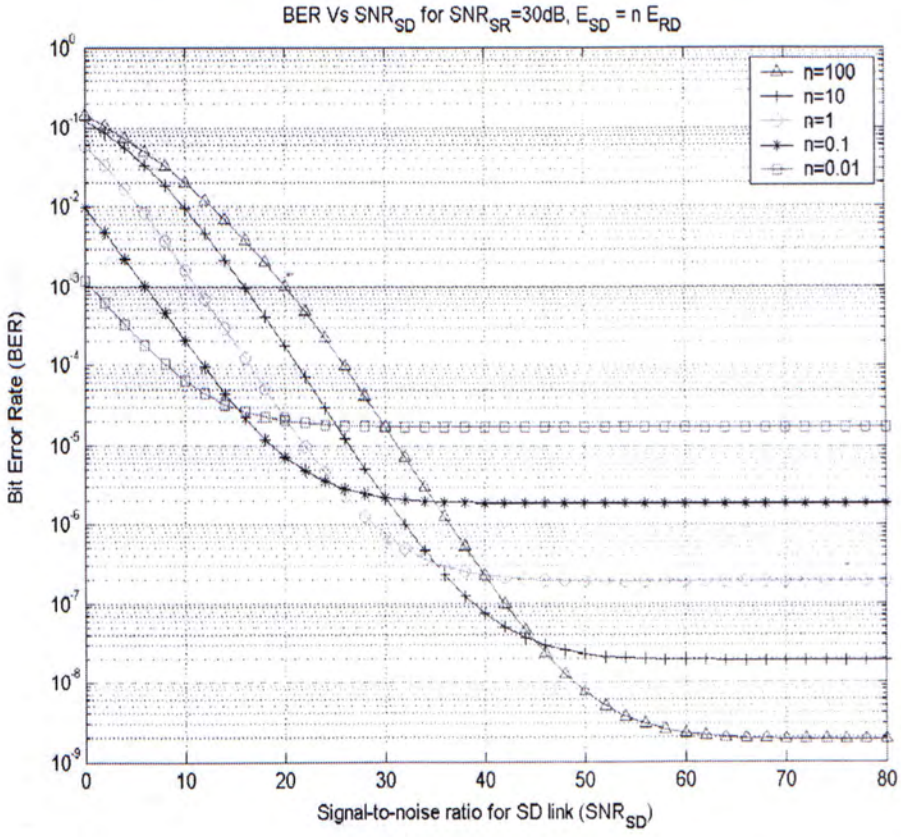

Figure 3.4: BER for static $R \rightarrow D$ link under different power imbalanced situations when $E_{SR}/N_0 = 30$dB.

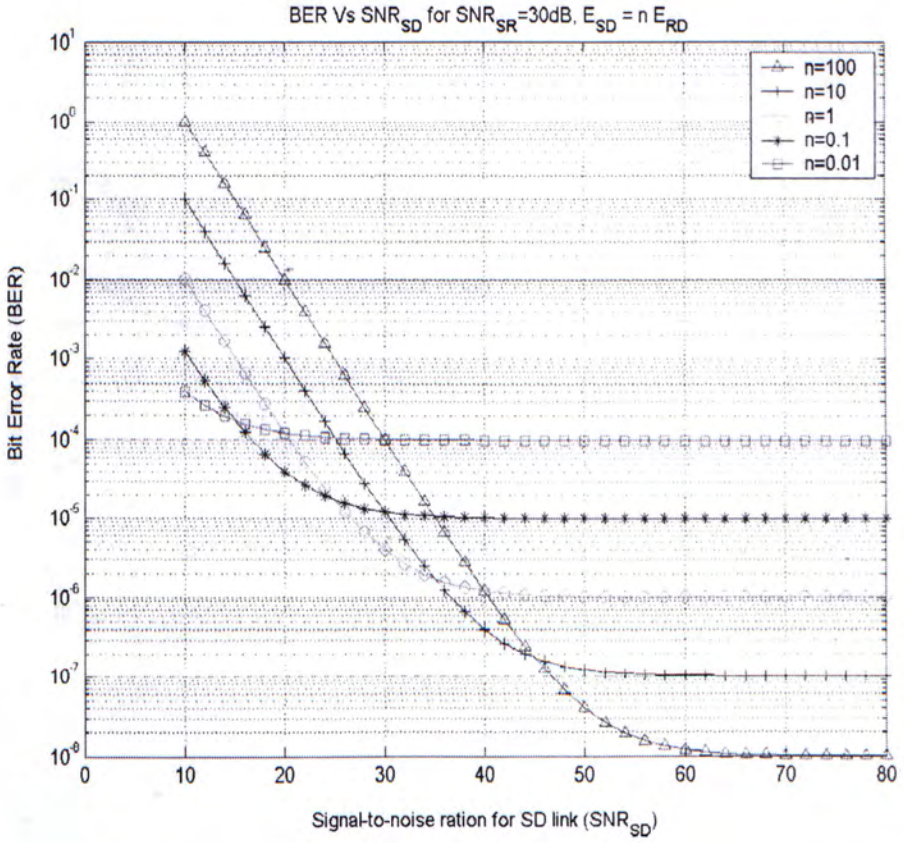

Figure 3.5: BER for fading $R \rightarrow D$ link under different power imbalanced situations when $E_{SR}/N_0 = 30\text{dB}$.

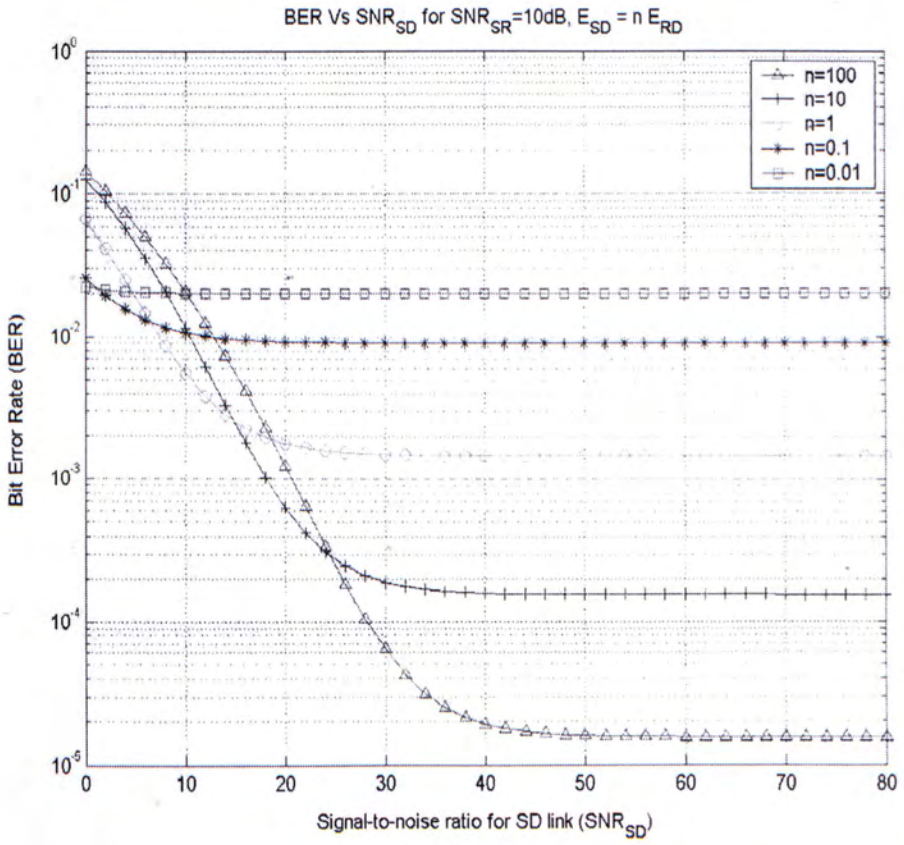

Figure 3.6: BER for static $R \rightarrow D$ link under different power imbalanced situations when $E_{SR}/N_0 = 10\text{dB}$.

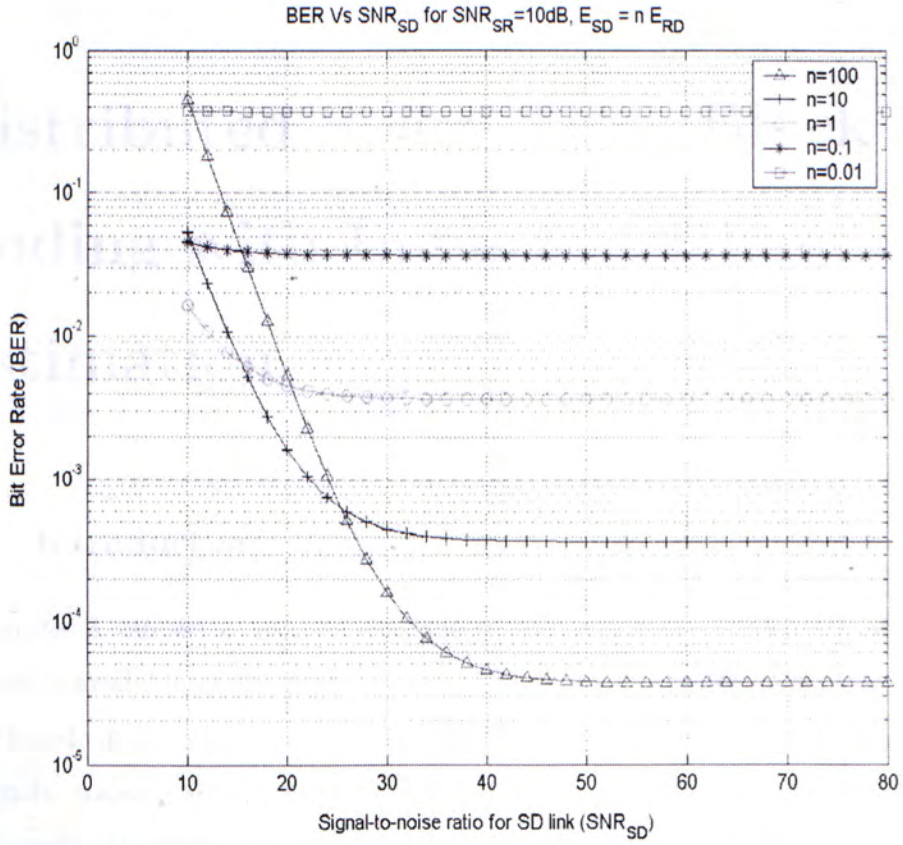

Figure 3.7: BER for fading $R \rightarrow D$ link under different power imbalanced situations when $E_{SR}/N_0 = 10$dB.

Chapter 4

Distributed Space-Time Block Coding with Imperfect Channel Estimation

4.1 Introduction

In chapter 3, our work assumes that the perfect knowledge of channel fading coefficients is available at the receiver side for the destination terminal. And we have mentioned, in practice, channel fading coefficients must be estimated. For static channels, training sequences or pilot symbols are common ways to estimate these coefficients. However, they are sometimes not accurate, thereby leading to performance degradation. In this chapter, we extend our investigation on bit-error-rate (BER) performance for the distributed STBC scheme with estimated channel state information (CSI), providing analytical closed-form expressions. The content of this chapter is mainly from [4].

4.2 System Model

The system model is the same as that shown in chapter 3 (Fig. 3.1). As a reminder, we adopt Alamouti's code matrix for transmission and the received signals are given as

$$r_1 = \alpha h_1 x_1 + \beta h_2 x_2 + n_1, \tag{4.1}$$

$$r_2 = -\alpha h_1 x_2^* + \beta h_2 x_1^* + n_2, \tag{4.2}$$

where α and β are defined as

$$\alpha = \sqrt{\frac{E_{SR}/N_0}{1 + E_{SR}/N_0 + E_{RD}/N_0}}\sqrt{E_{RD}}, \tag{4.3}$$

$$\beta = \sqrt{\frac{1 + E_{SR}/N_0}{1 + E_{SR}/N_0 + E_{RD}/N_0}}\sqrt{E_{SD}} \tag{4.4}$$

respectively.

4.3 BER Analysis

In this section, we derive the BER expressions for estimated channel state information (CSI), assuming binary phase shift keying (BPSK).

Here, the decoding process of x_1 and x_2 is based on the following statistics

$$\tilde{x_1} = \hat{h}_1^* r_1 + \hat{h}_2 r_2^* \tag{4.5}$$

$$\tilde{x_2} = \hat{h}_2^* r_1 - \hat{h}_1 r_2^* \tag{4.6}$$

where $\hat{h}_i$ is the estimate of h_i. We model $\hat{h}_i = h_i + z_i$, where z_i is defined as the channel estimation error. It is assumed to be an independent zero-mean complex Gaussian random variable with variance σ_z^2 and independent of h_i. Thus, the variance of $\hat{h}_i$ is: $\sigma_{\hat{h}}^2 = \sigma_h^2 + \sigma_z^2$, and the correlation of h_i and $\hat{h}_i$ is

$$\rho_{h\hat{h}} = \frac{1}{2}\frac{E[h_i \hat{h}_i^*]}{\sigma_h \sigma_{\hat{h}}} = \frac{\sigma_h}{\sigma_{\hat{h}}}. \tag{4.7}$$

Now that h_i and $\hat{h}_i$ are jointly Gaussian, conditioned on $\hat{h}_i$, h_i is a complex Gaussian random variable with mean $\rho\hat{h}_i$ and variance $\left(1-\rho_{h\hat{h}}^2\right)\sigma_h^2$ [16], where

$$\rho = \rho_{h\hat{h}}\left(\frac{\sigma_h}{\sigma_{\hat{h}}}\right) = \frac{\sigma_h^2}{\sigma_h^2+\sigma_z^2}. \tag{4.8}$$

Then, $h_i = \rho\hat{h}_i + d_i$, where d_i is an independent zero-mean complex Gaussian random variable with variance $\sigma_d^2 = \sigma_h^2\sigma_z^2/(\sigma_h^2+\sigma_z^2)$.

4.3.1 Non-fading $R \to D$ link

We start by considering that no power control is implemented. For the sake of simplifying the derivation, we assume $E_{SD} = nE_{RD}$, where n is a positive number. For $E_{SR}/N_0 \gg 1$, the closed-form BER expression which gives a bound before reaching an error floor can be found as (See Appendix C)

$$P(e) \approx \frac{1}{4}\left(1-\mu(\bar{\varepsilon_1})\right)^2\left(2+\mu(\bar{\varepsilon_1})\right) \tag{4.9}$$

where

$$\mu(\bar{\varepsilon_1}) = \sqrt{\frac{\bar{\varepsilon_1}}{2+\bar{\varepsilon_1}}}, \tag{4.10}$$

$$\bar{\varepsilon_1} = \frac{1}{\sqrt{n}}\frac{2\beta^2\cdot\Gamma}{(1+n)\alpha^2\cdot\nu\cdot\Gamma+1+\nu}. \tag{4.11}$$

Here, ν and Γ are denoted as the estimation error-to-signal ratio and effective signal-to-noise ratio respectively, where $\nu = \sigma_z^2/\sigma_h^2$ and $\Gamma = \sigma_h^2/\sigma_n^2$ [10]. The tight bound can be obtained for comparable E_{SD} and E_{RD} values. If power control is employed so that $E_{SD} = E_{RD}$, i.e. $n = 1$, then $\alpha = \beta = \omega$, where

$$\omega = \sqrt{\frac{E_{SR}/N_0\cdot E_{SD}}{1+E_{SR}/N_0+E_{RD}/N_0}}. \tag{4.12}$$

In this case, we are able to find an exact BER expression as (See Appendix C)

$$P(e) = \frac{1}{4}\left(1-\mu(\bar{\varepsilon})\right)^2\left(2+\mu(\bar{\varepsilon})\right) \tag{4.13}$$

where

$$\bar{\varepsilon} = \frac{2\omega^2\cdot\Gamma}{2\omega^2\cdot\nu\cdot\Gamma+1+\nu}. \tag{4.14}$$

4.3.2 Fading $R \rightarrow D$ link

For Rayleigh fading, assuming no power control, the BER expression becomes

$$P(e||h_{RD}|) \approx \frac{1}{4}\left(1-\mu(\bar{\varepsilon_1})\right)^2\left(2+\mu(\bar{\varepsilon_1})\right) \tag{4.15}$$

where

$$\bar{\varepsilon_1} = \frac{1}{\sqrt{n}}\frac{2\beta^2\cdot\Gamma}{(1+n)\alpha^2\cdot\nu\cdot\Gamma+1+\nu}\cdot|h_{RD}|^2, \tag{4.16}$$

$$\bar{\varepsilon_2} = \frac{2\beta^2\cdot\Gamma}{(1+n)\alpha^2\cdot\nu\cdot\Gamma+1+\nu}. \tag{4.17}$$

Under a high SNR assumption, (4.15) reduces to

$$P(e||h_{RD}|) \approx \frac{3}{4}\left(\bar{\varepsilon_1}\right)^{-2} \tag{4.18}$$

which yields the unconditional expression as

$$P(e) \approx -\frac{3n}{4}\left(\bar{\varepsilon_2}\right)^{-2}T(z). \tag{4.19}$$

where $T(z)$ is a truncated power series of $Ei(z)$ for small z. As in (3.35), a truncated power series representation given by (3.36) provides a good approximation to the above limit expression.

4.4 Numerical Results

In this section, we investigate the performance of imperfect channel estimation with and without power control, under the condition of $E_{SR}/N_0 = 30$dB.

With power control

Fig. 4.1 demonstrates the error flooring effect due to imperfect channel estimation. The closed-form BER expressions given by (4.13) and (4.19) are plotted for $n = 1$ and $\alpha = \beta = \omega$. For static $R \rightarrow D$ link, when the effective error-to-signal ratio, ν is at -20dB, the BER performance degrades rapidly compared with that of

perfect channel estimation. The error floor for $\nu = -20$dB appears about 10^{-4} while that for $\nu = -\infty$ is about 10^{-7} which levels off at a higher E_{SD}/N_0 value. For $\nu = -10$dB, the performance degradation becomes more severe resulting in an immediate error floor. For fading $R \rightarrow D$ link, we make similar observations noting an additional performance loss. In Fig. 4.1, we also include simulation results (illustrated by dashed lines) which confirm the accuracy of the derived analytical expressions. In short, channel estimation error causes a great impact on the BER performance. Even though the power of channel estimation error is 1/100 of the signal power, the BER performance for fading $R \rightarrow D$ link drops from 10^{-6} with perfect channel estimation to 10^{-3}. And, it is hard to maintain reliable communications when the power of channel estimation error is one-tenth of the signal power.

Without power control

For power imbalance, first, we are going to examine the tightness of our approximation of the closed-form BER expressions given by (4.9) and (4.19), which are plotted for $n = 10, 5, 2, 0.5, 0.2$. Figs. 4.2 and 4.3 show the BER performance under slight power imbalance. As expected, the curves for analytical expressions give tight bounds to simulation results in both cases. In Figs. 4.4 and 4.5, we see that the curves for analytical expressions start deviating, to a small extent, from simulation results when power imbalance becomes significant. When there is a great power difference in E_{SD} and E_{RD}, say 10dB, discrepancy becomes obvious in Fig. 4.6.

Second, unlike power imbalance for perfect channel estimation, the level of an error floor for imperfect channel estimation is altered when there is a any difference in E_{SD} and E_{RD}. And, the lowest level of error probability is achieved when $E_{SD} = E_{RD}$. Notice that for power imbalance for perfect channel estimation in chapter 3, the level of an error floor is higher when $E_{SD} \leq E_{RD}$ while that is lower when

$E_{SD} > E_{RD}$.

4.5 Summary

In this chapter, we have derived exact closed-form BER expressions for the distributed space-time block coded system by considering estimated channel state information (CSI) with and without power control. Our results indicate that the effect of imperfect channel estimation manifests itself as an error floor. For $E_{SD} = E_{RD}$, the lowest error floor and the optimal performance for imperfect channel estimation can be achieved. Under acceptable power imbalance, our analytical expressions provide tight bounds to simulation results.

□ **End of chapter.**

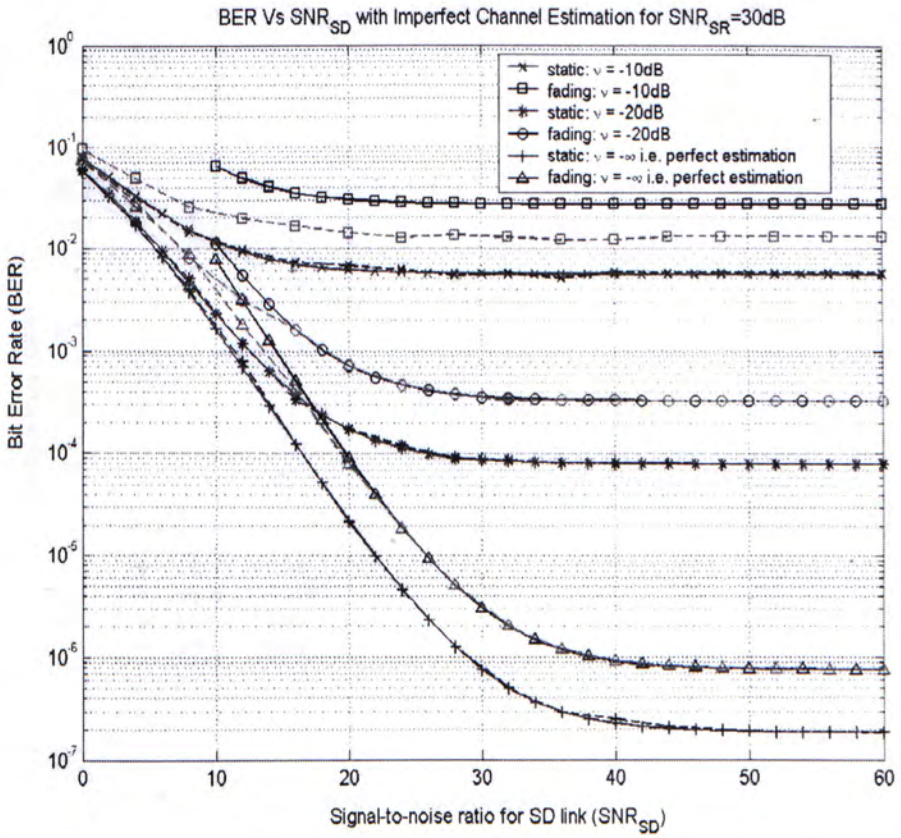

Figure 4.1: BER with imperfect channel estimation for static and fading $R \rightarrow D$ links. Analytical: Solid line; Simulation: Dashed line.

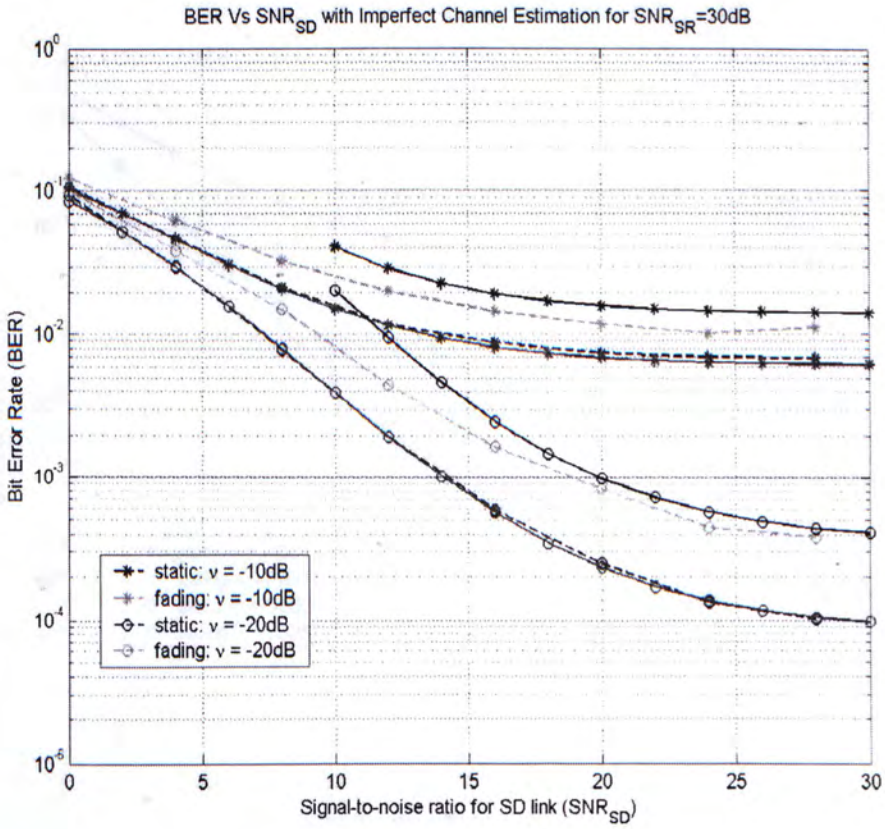

Figure 4.2: BER with imperfect channel estimation for static and fading $R \rightarrow D$ links under power imbalance, $n = 2$. Analytical: Solid line; Simulation: Dashed line.

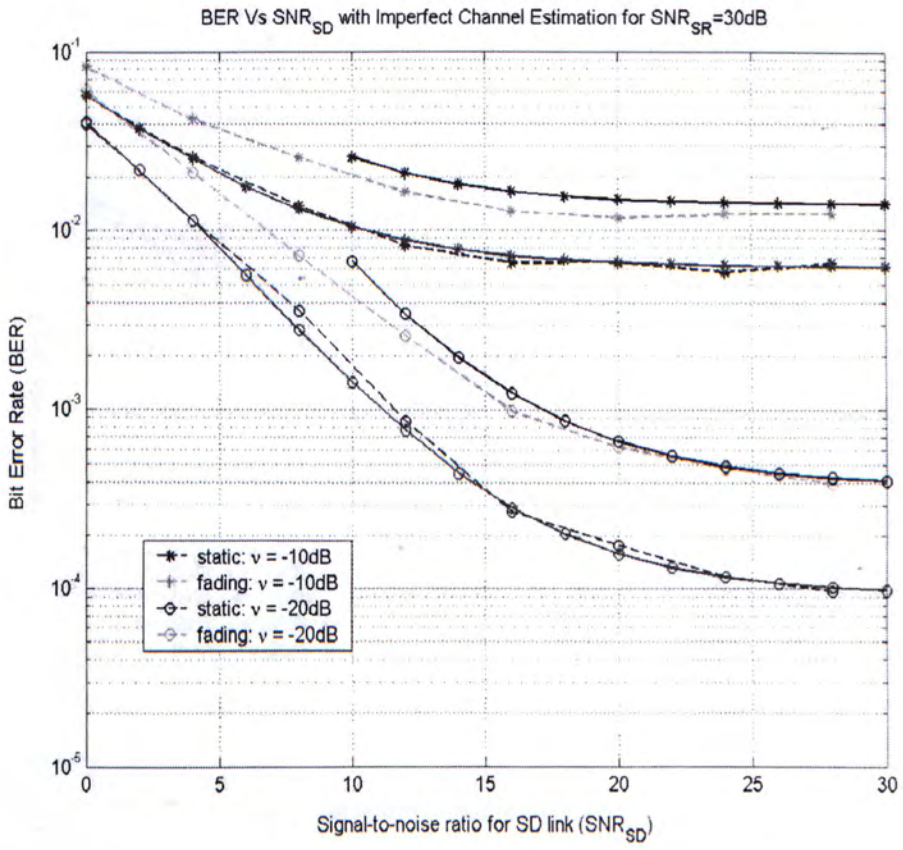

Figure 4.3: BER with imperfect channel estimation for static and fading $R \rightarrow D$ links under power imbalance, $n = 0.5$. Analytical: Solid line; Simulation: Dashed line.

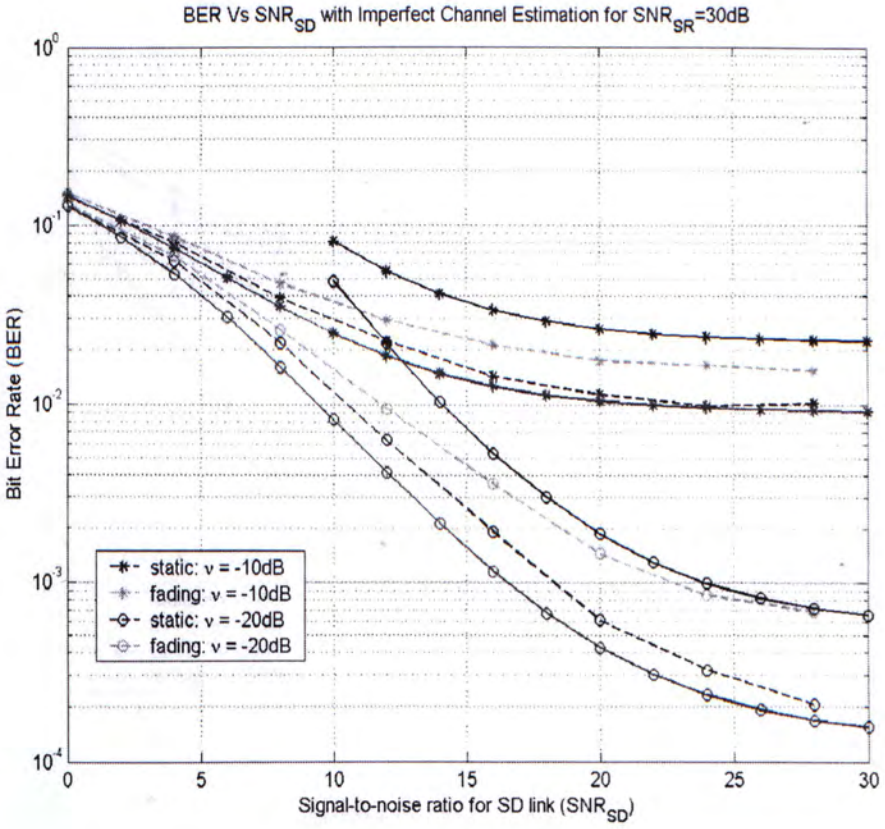

Figure 4.4: BER with imperfect channel estimation for static and fading $R \rightarrow D$ links under power imbalance, $n = 5$. Analytical: Solid line; Simulation: Dashed line.

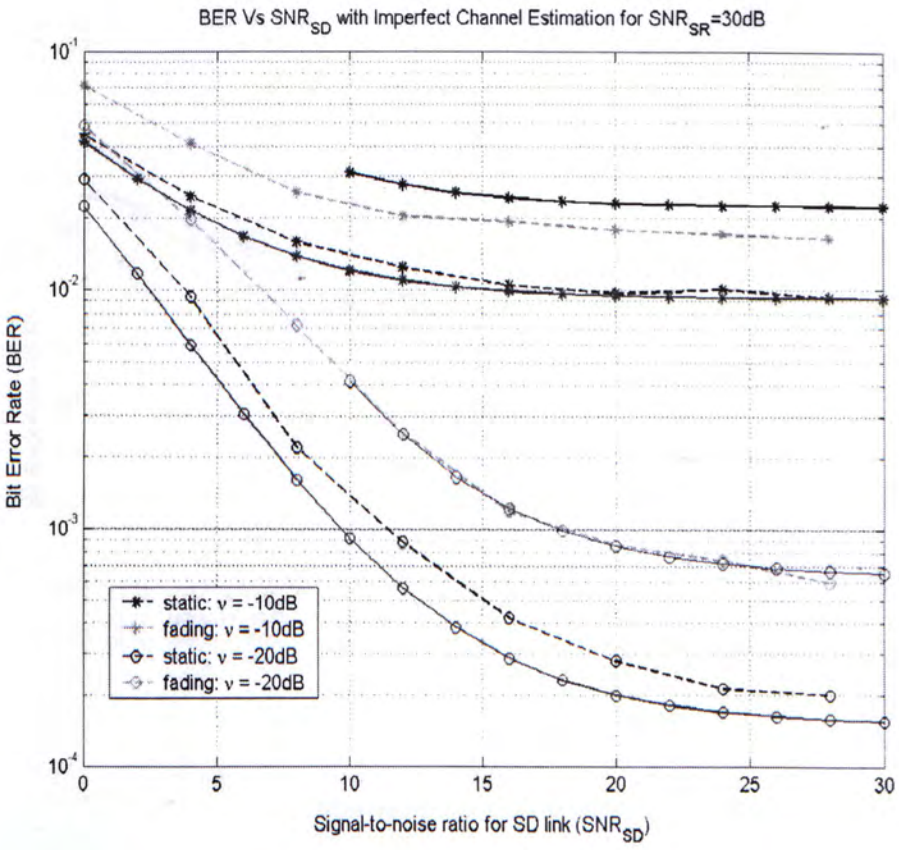

Figure 4.5: BER with imperfect channel estimation for static and fading $R \rightarrow D$ links under power imbalance, $n = 0.2$. Analytical: Solid line; Simulation: Dashed line.

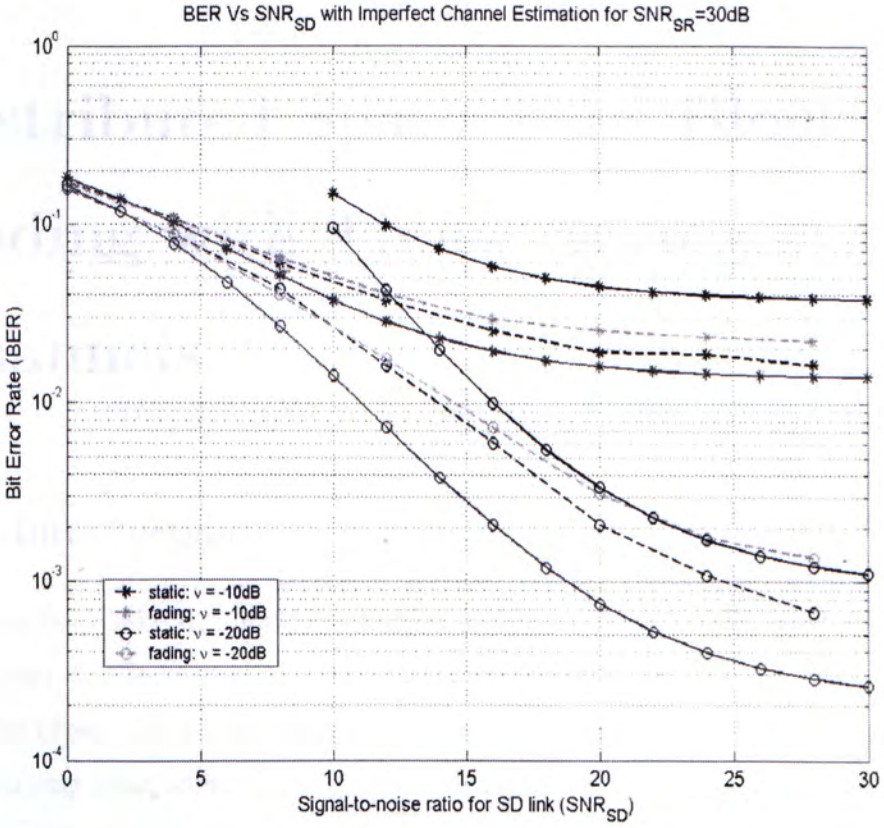

Figure 4.6: BER with imperfect channel estimation for static and fading $R \rightarrow D$ links under power imbalance, $n = 10$. Analytical: Solid line; Simulation: Dashed line.

Chapter 5

Distributed Space-Time Block Coding with Time-Varying Channels

5.1 Introduction

The practical issue of imperfect channel estimation for DSTBC has been studied in chapter 4. To extend the discussions on DSTBC, in this chapter, we study how the effect of time-varying channels alters the performance. Following Jakes' time-varying channel model [17], we investigate different reception schemes, encompassing maximum-likelihood receiver in [29], Alamouti's receiver, zero-forcing receiver, decision-feedback receiver and our newly considered detector called cooperative maximum-likelihood receiver. Also, we assess and compare their BER performances. In literature, the performance of conventional space-time block coding over time-varying channels has been investigated [29]. However, it is not realistic to assume that the channel coefficients can be estimated perfectly in fast time-varying channels or even uncorrelated channels. Some sort of channel estimation is necessary. In this chapter, first, we exploit the technique of pilot symbol

assisted modulation (PSAM) to estimate the time-varying channel coefficients and then study their BER performances by simulations. Second, under the assumption of ideal situations that the exact channel coefficients are available at the receiver, we derive closed-form expressions of zero-forcing and decision-feedback reception methods and discuss the discrepancies among all receivers.

5.2 System Model

The system model is the same as that shown in chapter 3 (Fig. 3.1). To model the time-varying channels, let $\tilde{h}_{SR}$, $\tilde{h}_{RD}$ and $\tilde{h}_{SD}$ denote the fading coefficients of $S \rightarrow R$, $R \rightarrow D$ and $S \rightarrow D$ links respectively during the second block period. Thus, the received signals are now given as

$$r_1 = \alpha h_1 x_1 + \beta h_2 x_2 + n_1, \tag{5.1}$$

$$r_2 = -\alpha \tilde{h}_1 x_2^* + \beta \tilde{h}_2 x_1^* + n_2 \tag{5.2}$$

where $\tilde{h}_1 = \tilde{h}_{SR}\tilde{h}_{RD}$ and $\tilde{h}_2 = \tilde{h}_{SD}$. In matrix form,

$$\begin{bmatrix} r_1 \\ r_2^* \end{bmatrix} = \begin{bmatrix} \alpha h_1 & \beta h_2 \\ \beta \tilde{h}_2^* & -\alpha \tilde{h}_1^* \end{bmatrix} \begin{bmatrix} x_1 \\ x_2 \end{bmatrix} + \begin{bmatrix} n_1 \\ n_2^* \end{bmatrix} \tag{5.3}$$

or

$$\mathbf{r} = \mathbf{H}\mathbf{x} + \mathbf{n}. \tag{5.4}$$

We employ Jakes' Model [17] for the above time-varying system and let ρ be the correlation between two successive channel realizations in two-symbol intervals. Then,

$$\rho = J_0 (2\pi f_D T) \tag{5.5}$$

where $J_0(.)$ is the zero-order Bessel function of the first kind, T is symbol interval and $f_D = \nu f_c / c$ is the maximum Doppler frequency, where ν is the vehicle speed in ms^{-1}. f_c is the carrier frequency, and c is the speed of light ($3 \times 10^8 ms^{-1}$). Throughout this chapter, we make the following assumptions:

- The pairs $(h_i, \tilde{h}_i)$ are independent for $i = 1, 2$.
- Temporally symmetric Rayleigh fading so that the correlation ρ between h_i and $\tilde{h}_i$ is the same for $i = 1, 2$, i.e. $E\left[h_i \tilde{h}_i^*\right] = \rho$.

In practice, as we are not able to obtain the perfect channel state information over time-varying channels, PSAM is the common way to estimate the time-varying channel coefficients.

5.3 Pilot Symbol Assisted Modulation (PSAM) for DSTBC

In most wireless applications, pilot symbols are inserted in the data frames for practical implementation of channel estimation. PSAM [3] achieves coherent demodulation in a fading environment by using pilot symbols to estimate the channel on a minimum-mean-squared-error (MMSE) basis. To the best of our understanding, PSAM has not been studied before in the context of a user cooperation scenario with time-varying channels.

In the considered PSAM scenario, the pilot symbols are sent separately over each link at different time slots. Specifically, in the time slot k, the source terminal S broadcasts the pilot symbol to the destination terminal D and the relay terminal R. In the time slot $k+1$, R transmits the received version of pilot symbol (after energy normalization) to D. There is no transmission from S to D within this period. These pilot symbols are placed at the front end, followed by $M-1$ data symbols in a data frame, where M is the size of data frame. At the receiver, D then extracts the L nearest pilot symbols in data frames and constructs two different sets that represent the pilot symbols received over the $S \rightarrow R \rightarrow D$ and $S \rightarrow D$ links. Subsequently, for each set of the received pilot symbols, the channel estimator is used to interpolate by incorporating a Wiener filter among the samples to construct a fading estimate for every symbol period.

Let p represent the pilot symbol, where $p^2 = 1$. The received pilot signals at the destination terminal are given as

$$r_{S\to D}^{k} = \beta h_2^k p + n^k \tag{5.6}$$

$$r_{S\to R\to D}^{k+1} = \alpha h_1^k p + n^{k+1} \tag{5.7}$$

where n^k and n^{k+1} are independent samples of complex Gaussian random variables with zero mean and variance of $N_0/2$ per dimension. Based on the received signals corresponding to pilot symbol transmissions, the destination terminal employs the Wiener filter to estimate the fading coefficients. As depicted in Fig. 5.1, $\lfloor L/2 \rfloor$ pilot symbols from the following frames and $\lfloor (L-1)/2 \rfloor$ pilot symbols from the previous and current frames are employed in this estimation. Defining

$$\bar{r}_{S\to D}^{k} = p \cdot r_{S\to D}^{k} \tag{5.8}$$

$$\bar{r}_{S\to R\to D}^{k+1} = p \cdot r_{S\to R\to D}^{k+1}, \tag{5.9}$$

and furthermore introducing the received signal vectors representing the L nearest received pilot symbols, i.e.

$$\bar{\mathbf{r}}_{S\to D} = [\bar{r}_{S\to D}^{-\lfloor (L-1)/2 \rfloor} \cdots \bar{r}_{S\to D}^{\lfloor L/2 \rfloor}]^T \tag{5.10}$$

$$\bar{\mathbf{r}}_{S\to R\to D} = [\bar{r}_{S\to R\to D}^{-\lfloor (L-1)/2 \rfloor} \cdots \bar{r}_{S\to R\to D}^{\lfloor L/2 \rfloor}]^T, \tag{5.11}$$

by using the Wiener filter, say for $S \to D$ link,

$$\mathbf{w}_{S\to D}(m) = [w_{S\to D}^{-\lfloor (L-1)/2 \rfloor}(m) \cdots w_{S\to D}^{\lfloor L/2 \rfloor}(m)] \tag{5.12}$$

and the corresponding fading estimate at the m^{th} symbol period is denoted by

$$\hat{h}_2(m) = \mathbf{w}_{S\to D}(m)\bar{\mathbf{r}}_{S\to D}. \tag{5.13}$$

With the knowledge of the second order channel statistics, the Wiener filter, which is regarded as the optimal interpolator, in the sense of MMSE, is the one that

minimizes

$$\varepsilon^2(m) = \frac{1}{2}E\left[|h_2(m) - \hat{h}_2(m)|^2\right] \tag{5.14}$$

$$= \frac{1}{2}E\left[|h_2(m) - \mathbf{w}_{S\to D}(m)\bar{\mathbf{r}}_{S\to D}|^2\right] \tag{5.15}$$

$$= \frac{1}{2}E\left[|h_2(m)|^2\right] + \frac{1}{2}E\left[\mathbf{w}_{S\to D}(m)\bar{\mathbf{r}}_{S\to D}\bar{\mathbf{r}}^*_{S\to D}\mathbf{w}^*_{S\to D}(m)\right]$$
$$- \frac{1}{2}E\left[h_2(m)\bar{\mathbf{r}}^*_{S\to D}\mathbf{w}^*_{S\to D}(m)\right] - \frac{1}{2}E\left[h_2^*(m)\mathbf{w}_{S\to D}(m)\bar{\mathbf{r}}_{S\to D}\right] \tag{5.16}$$

$$= \sigma^2_{h_2} + \mathbf{w}_{S\to D}(m)\mathbf{\Phi}_{\bar{\mathbf{r}}_{S\to D}\bar{\mathbf{r}}_{S\to D}}\mathbf{w}^*_{S\to D}(m)$$
$$- \mathbf{\Phi}_{h_2\bar{\mathbf{r}}_{S\to D}}(m)\mathbf{w}^*_{S\to D}(m) - \mathbf{w}_{S\to D}(m)\mathbf{\Phi}_{\bar{\mathbf{r}}_{S\to D}h_2}(m) \tag{5.17}$$

where

$$\mathbf{\Phi}_{h_2\bar{\mathbf{r}}_{S\to D}}(m) = \frac{1}{2}E\left[h_2(m)\bar{\mathbf{r}}^*_{S\to D}\right] = \Phi^*_{\bar{\mathbf{r}}_{S\to D}h_2}(m), \tag{5.18}$$

$$\mathbf{\Phi}_{\bar{\mathbf{r}}_{S\to D}\bar{\mathbf{r}}_{S\to D}} = \frac{1}{2}E\left[\bar{\mathbf{r}}_{S\to D}\bar{\mathbf{r}}^*_{S\to D}\right]$$
$$= \frac{1}{2}E\left[\begin{pmatrix} \bar{r}_{S\to D}^{-\lfloor (L-1)/2\rfloor} \\ \vdots \\ \bar{r}_{S\to D}^{\lfloor L/2\rfloor} \end{pmatrix}\left(\bar{r}_{S\to D}^{*-\lfloor (L-1)/2\rfloor}\cdots\bar{r}_{S\to D}^{*\lfloor L/2\rfloor}\right)\right]. \tag{5.19}$$

It can be obtained by solving

$$\frac{\partial}{\partial w^n_{S\to D}(m)}\varepsilon^2(m) = 0, \text{ for } n = -\lfloor (L-1)/2\rfloor, \ldots, \lfloor L/2\rfloor, \tag{5.20}$$

leading to $\mathbf{w}_{S\to D}(m)\mathbf{\Phi}_{\bar{\mathbf{r}}_{S\to D}\bar{\mathbf{r}}_{S\to D}} = \mathbf{\Phi}_{h_2\bar{\mathbf{r}}_{S\to D}}(m)$ (so called normal equation) or

$$\mathbf{w}_{S\to D}(m) = \mathbf{\Phi}_{h_2\bar{\mathbf{r}}_{S\to D}}(m)\mathbf{\Phi}^{-1}_{\bar{\mathbf{r}}_{S\to D}\bar{\mathbf{r}}_{S\to D}}. \tag{5.21}$$

So, the channel estimate for the m^{th} bit is

$$\hat{h}_2(m) = \mathbf{\Phi}_{h_2\bar{\mathbf{r}}_{S\to D}}(m)\mathbf{\Phi}^{-1}_{\bar{\mathbf{r}}_{S\to D}\bar{\mathbf{r}}_{S\to D}}\bar{\mathbf{r}}_{S\to D}. \tag{5.22}$$

Defining $J_k \triangleq J_0(2\pi k f_d T)$,

$$\phi_{h_2\bar{\mathbf{r}}_{S\to D}}(m,n) = \frac{1}{2}E\left[h_2(m)\hat{h}_2(nM)\right] \tag{5.23}$$

$$= \sigma^2_{h_2} J_{m-nM} \tag{5.24}$$

$$\phi_{\bar{\mathbf{r}}_{S\to D}\bar{\mathbf{r}}_{S\to D}}(m,n) = \frac{1}{2}E\left[\hat{h}_2(mM)\hat{h}_2(nM)\right] \tag{5.25}$$

$$= \begin{cases} \sigma^2_{h_2} + N_0, & \text{if } m = n \\ \sigma^2_{h_2} J_{(m-n)M} & \text{else} \end{cases} \tag{5.26}$$

The corresponding mean-square-error (MSE) is

$$\varepsilon^2(m) = \sigma^2_{h_2} - \mathbf{\Phi}_{h_2\bar{\mathbf{r}}_{S\to D}}(m)\mathbf{\Phi}^{-1}_{\bar{\mathbf{r}}_{S\to D}\bar{\mathbf{r}}_{S\to D}}\mathbf{\Phi}_{\bar{\mathbf{r}}_{S\to D}h_2}(m) \tag{5.27}$$

Similarly, the channel estimate $\hat{h}_1(m)$ for $S \to R \to D$ link is given by

$$\hat{h}_1(m) = \mathbf{\Phi}_{h_1\bar{\mathbf{r}}_{S\to R\to D}}(m)\mathbf{\Phi}^{-1}_{\bar{\mathbf{r}}_{S\to R\to D}\bar{\mathbf{r}}_{S\to R\to D}}\bar{\mathbf{r}}_{S\to R\to D}. \tag{5.28}$$

With these channel estimates, we can then construct different receivers and analyze their performances in terms of BER.

5.4 Reception Methods

In this section, we examine five reception methods for signals detection. They are maximum-likelihood receiver in [29], cooperative maximum-likelihood receiver, Alamouti's receiver, zero-forcing receiver, decision-feedback receiver, assuming binary phase shift keying (BPSK). Here, we denote $g_1, g_2, \tilde{g}_1$ and $\tilde{g}_2$ as the estimated values of $h_1, h_2, \tilde{h}_1$ and $\tilde{h}_2$ respectively.

5.4.1 Maximum-Likelihood Detection (ML) in [29]

In the presence of AWGN, the maximum-likelihood (ML) detection is equivalent to:

$$\arg\min_{\mathbf{x}} \|\mathbf{r} - \hat{\mathbf{H}}\mathbf{x}\|^2 \tag{5.29}$$

where

$$\hat{\mathbf{H}} = \begin{bmatrix} \alpha g_1 & \beta g_2 \\ \beta \tilde{g}_2^* & -\alpha \tilde{g}_1^* \end{bmatrix}. \tag{5.30}$$

Let $\mathbf{R} = \hat{\mathbf{H}}^* \hat{\mathbf{H}}$, where

$$\mathbf{R} = \begin{bmatrix} \alpha^2|g_1|^2 + \beta^2|\tilde{g}_2|^2 & \alpha\beta g_1^* g_2 - \alpha\beta \tilde{g}_1^* \tilde{g}_2 \\ \alpha\beta g_1 g_2^* - \alpha\beta \tilde{g}_1 \tilde{g}_2^* & \alpha^2|\tilde{g}_1|^2 + \beta^2|g_2|^2 \end{bmatrix}. \tag{5.31}$$

Now that $\mathbf{R}$ is Hermitian, we can express $\mathbf{R} = \mathbf{G}^*\mathbf{G}$ by the Cholesky factorization, where G is given as

$$\mathbf{G} = \frac{1}{\sqrt{\alpha^2|\tilde{g}_1|^2 + \beta^2|g_2|^2}} \cdot \begin{bmatrix} |\alpha^2 g_1 \tilde{g}_1^* + \beta^2 g_2 \tilde{g}_2^*| & 0 \\ \alpha\beta g_1 g_2^* - \alpha\beta \tilde{g}_1 \tilde{g}_2^* & \alpha^2|\tilde{g}_1|^2 + \beta^2|g_2|^2 \end{bmatrix}. \tag{5.32}$$

Then, we can convert (5.29) into

$$\arg\min_{\mathbf{x}} \ |\mathbf{z} - \mathbf{G}\mathbf{x}\|^2 \tag{5.33}$$

where

$$\mathbf{z} = \mathbf{G}^{-*}\hat{\mathbf{H}}^*\mathbf{r} \tag{5.34}$$

by multiplying (5.29) by the unitary matrix $\mathbf{G}^{-*}\hat{\mathbf{H}}^*$.The equation (5.34) actually represents the whitening matched filter at the receiver. Multiplying both sides in (5.4) by $\mathbf{G}^{-*}\hat{\mathbf{H}}^*$ gives the following:

$$\mathbf{z} = \mathbf{G}\mathbf{x} + \mathbf{w} \tag{5.35}$$

where $z = [z_1, z_2]^T$ and $\mathbf{w}$, which is the white Gaussian noise, has the same statistical properties of $\mathbf{n}$.

5.4.2 Cooperative Maximum-Likelihood Detection (CML)

In our transmission protocol of interest, in the first signaling period, if the destination D is idle, it may receive some portions of the signal sent from the source S. Thus, the received signals can be given by

$$r_{11} = \sqrt{E_{SD}} h_2 x_1 + n_{11}, \tag{5.36}$$

$$r_{12} = \alpha h_1 x_1 + \beta h_2 x_2 + n_{12}, \tag{5.37}$$

$$r_{21} = -\sqrt{E_{SD}} \tilde{h}_2 x_2^* + n_{21}, \tag{5.38}$$

$$r_{22} = -\alpha \tilde{h}_1 x_2^* + \beta \tilde{h}_2 x_1^* + n_{22} \tag{5.39}$$

and the cooperative maximum-likelihood (CML) detection is as follows

$$\arg \min_{\mathbf{x}} \|\mathbf{r} - \hat{\mathbf{P}}\mathbf{x}\|^2 \tag{5.40}$$

where

$$\hat{\mathbf{P}} = \begin{bmatrix} \sqrt{E_{SD}} g_2 & 0 \\ \alpha g_1 & \beta g_2 \\ 0 & -\sqrt{E_{SD}} \tilde{g}_2^* \\ \beta \tilde{g}_2^* & -\alpha \tilde{g}_1^* \end{bmatrix}. \tag{5.41}$$

This time, all the signals sent either from the source or from the relay or both can be taken into account for demodulation at the destination. In order words, we make use of all available information. And, the performance of CML detection is expected to be better than that of ML detection due to the diversity gain if not all the channels are fully correlated. For the sake of simplicity, we ignore the power gains and consider the following code matrix

$$\mathcal{C} = \begin{bmatrix} 0 & x_1 & 0 & 0 \\ x_1 & x_2 & 0 & 0 \\ 0 & 0 & 0 & -x_2^* \\ 0 & 0 & -x_2^* & x_1^* \end{bmatrix} \tag{5.42}$$

in

$$\begin{bmatrix} r_{11} \\ r_{12} \\ r_{21} \\ r_{22} \end{bmatrix} = \begin{bmatrix} 0 & x_1 & 0 & 0 \\ x_1 & x_2 & 0 & 0 \\ 0 & 0 & 0 & -x_2^* \\ 0 & 0 & -x_2^* & x_1^* \end{bmatrix} \begin{bmatrix} h_1 \\ h_2 \\ \tilde{h}_1 \\ \tilde{h}_2 \end{bmatrix} + \begin{bmatrix} n_{11} \\ n_{12} \\ n_{21} \\ n_{22} \end{bmatrix}, \tag{5.43}$$

If all channels are independent, the above code matrix $\mathcal{C}$ can achieve third order diversity as its rank equals three. In order to maximize the diversity benefit or in other words, to obtain the quasi-independent channels, we separate the transmission stream into two parts. Assume that the frame size (M) is 5. The situation is depicted in Fig. 5.2. At the receiver, the signals are recombined before entering the CML detector.

5.4.3 Alamouti's Receiver (AR)

This detection scheme used to combine and decode the symbols is shown below:

$$\hat{x}_1 = sign(g_1^* r_1 + g_2 r_2^*) \tag{5.44}$$

$$\hat{x}_2 = sign(\tilde{g}_2^* r_1 - \tilde{g}_1 r_2^*) \tag{5.45}$$

As it simply does nothing with the received signals, say, to suppress the noise, it is expected to be the worst reception scheme.

5.4.4 Zero-forcing Linear Detection (ZF)

The aim of this detection is to force the crosstalk to zero:

$$\mathbf{y} = \mathbf{Cr} \tag{5.46}$$

A linear operation $\mathbf{C}$ tries to make a decision on x_i based on y_i, for $i = 1, 2$. That means, $\mathbf{C}\hat{\mathbf{H}}$ is a nonnegative diagonal matrix or $\mathbf{C} = \mathbf{A}\hat{\mathbf{H}}^{-1}$ for some nonnegative

diagonal matrix $\mathbf{A}$. To keep the noise variance the same, it is easy to show that

$$\mathbf{C} = \frac{|\alpha^2 g_1 \tilde{g}_1^* + \beta^2 g_2 \tilde{g}_2^*|}{\alpha^2 g_1 \tilde{g}_1^* + \beta^2 g_2 \tilde{g}_2^*} \mathbf{M} \begin{bmatrix} \alpha \tilde{g}_1^* & \beta g_2 \\ \beta \tilde{g}_2^* & -\alpha g_1 \end{bmatrix} \tag{5.47}$$

where

$$\mathbf{M} = \begin{bmatrix} \sqrt{\alpha^2 |\tilde{g}_1|^2 + \beta^2 |g_2|^2} & 0 \\ 0 & \sqrt{\alpha^2 |g_1|^2 + \beta^2 |\tilde{g}_2|^2} \end{bmatrix} \tag{5.48}$$

and

$$\mathbf{A} = |\alpha^2 g_1 \tilde{g}_1^* + \beta^2 g_2 \tilde{g}_2^*| \, \mathbf{M}. \tag{5.49}$$

Hence, it is easily verified that $\mathbf{A}\mathbf{R}^{-1}\mathbf{A}$ has ones on the diagonal so that the noise variance does not change. Substituting (5.47) and (5.4) into (5.46) gives

$$\mathbf{y} = \mathbf{A}\mathbf{x} + \tilde{\mathbf{n}} \tag{5.50}$$

where $\tilde{\mathbf{n}} = \mathbf{A}\mathbf{H}^{-1}\mathbf{w}$, $\tilde{n}_1$ and $\tilde{n}_2$ are zero-mean complex Gaussian with variance $N_0/2$ per dimension. The suboptimal decision on $\hat{x}_i$ regarding to x_i is obtained by quantizing y_i only, for $i = 1, 2$.

5.4.5 Decision-feedback Detection (DF)

From (5.32), there is only one symbol x_1 contributing to the first received signal z_1 in (5.35). By quantizing z_1, we can obtain a suboptimal decision $\hat{x}_1$. We assume this detection is correct and then subtract it off in z_2. Then, we can quantize the resulting difference, denoted by D, to obtain $\hat{x}_2$, where

$$D = z_2 - \frac{\alpha\beta \left(g_1 g_2^* - \tilde{g}_1 \tilde{g}_2^* \right)}{\sqrt{\alpha^2 |\tilde{g}_1|^2 + \beta^2 |g_2|^2}} \hat{x}_1 \tag{5.51}$$

In other words, the decoded symbols are

$$\hat{x}_1 = sign\left(z_1\right) \tag{5.52}$$

$$\hat{x}_2 = sign\left(D\right) \tag{5.53}$$

For ideal but unrealistic cases, we simply substitute $h_1, h_2, \tilde{h}_1$ and $\tilde{h}_2$ into $g_1, g_2, \tilde{g}_1$ and $\tilde{g}_2$ respectively. If we have the exact knowledge of channel state information, then we can derive the closed-form BER expressions for the ZF and DF receivers.

5.5 BER Analysis for Time-varying Channels

Assuming that the receiver can obtain the perfect knowledge of channel state information, consider the BER expressions for the time-varying channels. First, we derive the BER expressions for the quasi-static channels ($\rho = 1$). Second, we derive BER expressions for the uncorrelated channels ($\rho = 0$). Lastly, we consider the general channel with arbitrary ρ. Notice that for ML, CML and AR detections, it is not obvious to obtain the exact closed-form BER expressions. In this section, we mainly consider the BER performances of the other two detectors, ZF detector and DF detector.

5.5.1 Quasi-Static Channels ($\rho = 1$)

If $\rho = 1$, in fact, all the aforementioned detectors, except CML, have the same performance even though the underlying operations are different among them. In essence, if the channel is quasi-static, $\tilde{h}_i = h_i$, for $i = 1, 2$. Considering ML, (5.31) becomes

$$\mathbf{R} = \left(\alpha^2|h_1|^2 + \beta^2|h_2|^2\right)\mathbf{I}_2 \tag{5.54}$$

where $\mathbf{I}_2$ is a 2x2 identity matrix, and (5.35) becomes

$$\mathbf{z} = \sqrt{\alpha^2|h_1|^2 + \beta^2|h_2|^2}\,\mathbf{x} + \mathbf{n}. \tag{5.55}$$

Considering DF, as the second term in (5.51) vanishes, the received signals of DF becomes (5.55). For ZF, (5.49) becomes

$$\mathbf{A} = \sqrt{\alpha^2|h_1|^2 + \beta^2|h_2|^2}\,\mathbf{I}_2 \tag{5.56}$$

and (5.50) reduces to (5.55). The case of AR is of the same story. Thus, all of these 4 detectors have the same performance, i.e. Bit-error-rate (BER). The closed-form BER expressions are obtained in [4] and given in chapter 4. CML detection is expected to have an advantage because of the power gain.

5.5.2 ZF: Uncorrelated Channel ($\rho = 0$)

Consider the ZF linear detector. Due to the symmetry of the channel, we focus on the symbol x_1 only. From (5.50), we have

$$y_1 = \left(\frac{|\alpha^2 h_1 \tilde{h}_1^* + \beta^2 h_2 \tilde{h}_2^*|}{\sqrt{\alpha^2 |\tilde{h}_1|^2 + \beta^2 |h_2|^2}} \right) x_1 + \tilde{n}_1 \tag{5.57}$$

and its unconditional BER is $\mathrm{Q}\left(\sqrt{2a}\right)$, where

$$a = \frac{|\alpha^2 h_1 \tilde{h}_1^* + \beta^2 h_2 \tilde{h}_2^*|^2}{\alpha^2 |\tilde{h}_1|^2 + \beta^2 |h_2|^2} \cdot \frac{1}{N_0} \tag{5.58}$$

Let

$$v_1 = \frac{\alpha \tilde{h}_1}{\sqrt{\alpha^2 |\tilde{h}_1|^2 + \beta^2 |h_2|^2}}, \tag{5.59}$$

$$v_2 = \frac{\beta h_2^*}{\sqrt{\alpha^2 |\tilde{h}_1|^2 + \beta^2 |h_2|^2}}, \text{ and} \tag{5.60}$$

$$Y = v_1^* u_1 + v_2^* u_2 \tag{5.61}$$

where $\mathbf{u} = [u_1 \; u_2]^T = [\alpha h_1 \; \beta \tilde{h}_2^*]^T$. In fact, we can interpret Y as a projection of $\mathbf{v}^*\mathbf{u}$ of $\mathbf{u}$ in the direction of the independent unit vector $\mathbf{v} = [v_1 \; v_2]^T$. If $E_{SR}/N_0 \gg 1$ and an appropriate power control is employed, i.e. $\alpha = \beta$, we consider both non-fading and fading $R \to D$ links.

ZF: Non-fading $R \to D$ link

If $R \to D$ link is static (i.e. $h_{RD} = 1$), $\mathbf{u}$ is then symmetric. Since $\mathbf{u}$ and $\mathbf{v}$ are independent, Y is also independent of $\mathbf{v}$. By choosing $\mathbf{v} = [1 \; 0]^T$, then $a = \bar{\gamma}|h_1|^2$,

where $\bar{\gamma} = \alpha^2/N_0$. Thus, by using the method in [5], the BER is well-known and given as

$$P(e) = \frac{1}{2}\left(1 - \sqrt{\frac{\bar{\gamma}}{1+\bar{\gamma}}}\right) \tag{5.62}$$

ZF: Rayleigh fading $R \to D$ link

If $R \to D$ link is subject to Rayleigh fading, $\mathbf{u}$ is no longer symmetric. Then, the exact BER can be found by computing

$$P(e) = \int Q(\sqrt{2a}) f_p(p) dp \tag{5.63}$$

where $p = (h_1, \tilde{h}_1, h_2, \tilde{h}_2)$. Unfortunately, (5.63) does not give an explicit closed-form expression. Instead, we obtain an approximation by assuming that $\mathbf{u}$ is symmetric. Then, under high SNR, the unconditional BER expression is given as

$$P(e||h_{RD}|) \approx \left(4\bar{\gamma}|h_{RD}|^2\right)^{-1} \tag{5.64}$$

yielding

$$P(e) \approx (-4\bar{\gamma})^{-1} T(z) \tag{5.65}$$

5.5.3 ZF: General Channel

For an aribitary $\rho \in [0, 1]$, let ζ_1 and ζ_2 be independent random variables and their distributions are identically distributed as $\tilde{h}_1$ and h_2 respectively. In other words,

$$h_1 = \rho\tilde{h}_1 + \sqrt{1-\rho^2}\,\zeta_1, \tag{5.66}$$

$$\tilde{h}_2 = \rho h_2 + \sqrt{1-\rho^2}\,\zeta_2. \tag{5.67}$$

Using the similar method in [29] and employing an appropriate power control, we obtain the BER expressions for both static and fading $R \to D$ links.

ZF: Non-fading $R \to D$ link

If $h_{RD} = 1$, then (See Appendix D)

$$P(e) = \frac{\rho^2}{2}\left(1 - \frac{3+2\bar{\gamma}}{2+2\bar{\gamma}}\sqrt{\frac{\bar{\gamma}}{1+\bar{\gamma}}}\right) + \frac{1-\rho^2}{2}\left(1 - \sqrt{\frac{\bar{\gamma}}{1+\bar{\gamma}}}\right). \tag{5.68}$$

ZF: Rayleigh fading $R \to D$ link

Under high SNR assumption, we obtain the following approximation of its BER expression:

$$P(e) \approx \left(\rho^2\left(-4\bar{\gamma}^2\right)^{-1} + (1-\rho^2)\left(-4\bar{\gamma}\right)^{-1}\right) T(z). \tag{5.69}$$

5.5.4 DF: General Channel

For the DF detector, we can approximate its BER by assuming that the decision on $\hat{x}_1$ is correct. We consider the error probability of the first symbol x_1. As the received signal is exactly the same as that of the ZF detector, its $P_1(e)$ is given by (5.68) or (5.69). For the second symbol x_2, under the above assumption that the decoded $\hat{x}_1$ is correct so that the contribution due to x_1 can be subtracted off in (5.51), quantizing D or z_2 will give the decoded $\hat{x}_2$, where

$$D = \sqrt{\alpha^2|\tilde{h}_1|^2 + \beta^2|h_2|^2}\; x_2 + w_2 \tag{5.70}$$

and $P_2(e)$ is given by (3.32) or (3.35). Thus, for an equiprobable symbol transmission and $\alpha = \beta$, we can now approximate the BER performance by the following expressions:

DF: Non-Fading $R \to D$ link

$$P(e) \approx \frac{1+\rho^2}{4}\left(1 - \frac{3+2\bar{\gamma}}{2+2\bar{\gamma}}\sqrt{\frac{\bar{\gamma}}{1+\bar{\gamma}}}\right) + \frac{1-\rho^2}{4}\left(1 - \sqrt{\frac{\bar{\gamma}}{1+\bar{\gamma}}}\right) \tag{5.71}$$

DF: Rayleigh fading $R \to D$ link

$$P(e) \approx \left(\frac{1+\rho^2}{2}\left(-4\bar{\gamma}^2\right)^{-1} + \frac{1-\rho^2}{2}\left(-4\bar{\gamma}\right)^{-1}\right) T(z) \tag{5.72}$$

5.6 Numerical Results

In this section, we mainly focus on the numerical results with fading $R \rightarrow D$ link only. We start considering and discussing the performance of different receivers over time-varying channels with PSAM. First, we choose the frame size $M = 7$ and the number of interpolation coefficients $L = 5$. For CML detection, we separate transmitted signals into two parts so as to increase the independency of the channels while for the other schemes, the transmitted signals are closely packed as sparse packing does not improve the BER performance. For $E_{SR}/N_0 = 30$dB and the balanced links, i.e. $E_{SD} = E_{RD}$, unlike the results obtained in [29], in our simulations, most detectors attain nearly the same performance in terms of BER. The simulation results for different settings are plotted. For $f_D T = 0.03$ or $\rho = 0.99$, the performance is shown in Fig. 5.3. We observe that mainly ascribed to diversity gain, CML detection defeats the others by about 4dB. On the other hand, the performances of the other reception methods do not differ from each other. Fig. 5.4 shows that for $f_D T = 0.05$ or $\rho = 0.9755$, again, ZF, AR, DF and ML detections have the similar performance but they perform worse than before. CML detection still outperforms the others by about 4dB as its diversity gain can compensate the effect of channel estimation error to a certain extent. With practical consideration in time-varying channels, by employing PSAM, most detectors have the similar performances, which contradicts to the results obtained in [29] by assuming perfect channel state information available at the receiver.

For $\rho = 0.95$ ($f_D T = 0.0716$) and $\rho = 0.9037$ ($f_D T = 0.1$), their performances become more worse due to the accumulated errors in channel estimation over fast time-varying channels, which are plotted in Figs. 5.5 and 5.6. In these cases, the CML detector is the best one among all, which prevails over the others by about 5dB. As regards the case for $\rho = 0.9037$, we can see an immediate error floor, though CML detection has a diversity benefit. Let consider the case of $M = 5$ and $L = 5$.

Data Rate (R)	Doppler Value ($f_D T$)	Correlation Value (ρ)
38.4k	0.00625	0.99961
64k	0.00375	0.99986
128k	0.001875	0.99997

Table 5.1: The table showing the data rates with the corresponding Doppler values and correlation values at $f_c = 2.4$G Hz and $\nu = 30$m/s.

For $\rho = 0.9755$, the performance is similar to that of $M = 5$ and $L = 5$, which is shown in Fig. 5.7. But for $\rho = 0.9037$, unlike the case of $M = 5$ and $L = 5$, all detectors achieve relatively better performances that are shown in Fig. 5.8. The main reason is that the frame size is smaller and hence the ratio of pilot symbol to data symbol is higher. Thus, the channel estimation is relatively better. And, Fig. 5.9 shows the performance for $\rho = 0.85$ ($f_D T = 0.1257$). The CML detector performs the best but the immediate error is observed at around 10^{-1}. In fact, under such a time-varying ambience, it cannot maintain reliable communications. In theory, yet, if we have better channel estimates, different detectors can be distinguished. Nevertheless, it is hard to obtain good estimates in a fast time-varying environment. For example, when $M = 5$ and $L = 5$, at the level of $E_{SD}/N_0 = 16$dB, the mean square error (MSE) for $\rho = 0.99$ is about 0.007 while that for $\rho = 0.85$ is about 0.13, and the ratio of the square root of their MSE is about 4-fold, thereby causing a great impact on BER.

Discussion

In our daily life, most applications operate over slow time-varying conditions. For example, for some 3G applications, their data rates (R) are, say 38.4k, 64k, and 128k in bits per second and they usually operate at 2.4G Hz. If the vehicle speed is 30 m/s, then the corresponding Doppler values ($f_D T$) and correlation values (ρ) are listed in Table 5.1. From the table, there are two implications. One is that most current applications are not vulnerable to time-varying channels. Second, from our

Data Rate (R)	Doppler Value ($f_D T$)	Correlation Value (ρ)
200k	0.1	0.9037
400k	0.05	0.9755
1M	0.02	0.9961

Table 5.2: The table showing the data rates with the corresponding Doppler values and correlation values at $f_c = 30$G Hz and $\nu = 200$m/s.

previous results, with PSAM, using any of the above receivers is feasible as they have similar performances. But for our future applications, some of them may suffer from time-varying channels. In Table 5.2, we consider some settings of future applications: The vehicle speed is 200 m/s and the carrier frequency is 30G Hz. We see that for these applications, the time-varying channels may cause a great impact on the performance. In such a fast time-varying environment, exploiting CML detection will help maintain reliable communications to a certain extent.

Next, we compare the BER performance of different reception schemes by assuming that perfect knowledge of channel state information is available at the receiver. For ML, CML and AR detections, we rely on computer simulations while we plot the analytical expressions for ZF and DF detectors. As the derivation of BER expression of DF is based on the assumption that the symbol $\hat{x}_1$ is correctly decoded, we first compare the BER of its analytical results with its simulation results for $\rho = 0.5,\ 0.9755$. In Fig. 5.10, obviously, the BER expressions (5.71) and (5.72), for static and fading $R \rightarrow D$ links respectively, provide tight bounds to the simulation results. Then, we are going to compare these five reception schemes. With perfect channel knowledge, different receivers behave differently. For $\rho = 0.9755$ in Fig. 5.11, CML detection prevails over the others by at least 5dB due to the third order diversity. ML lags behind. DF and ZF have similar performances but the former one performs better by about 1dB. The worst one is AR, which is the most

vulnerable. The same trend is observed in Fig. 5.12 for $\rho = 0.5$. The performances of CML and ML detections are more or less the same as that are shown in Fig. 5.11 but the other detections suffer a lot from the fast time-varying environment. In general, the influence of time-varying channels induces the error floor.

Last, we make a comparison of the performances for channel estimation by PSAM and that for perfect channel estimation. For $\rho = 0.9755$, the BER performances of two groups of curves are plotted in Fig. 5.13. As seen, there is a noticeable gap between these two sets of curves. Only the performance of the CML detector with PSAM is comparable to that of the ZF and DF detectors with perfect CSI. This reveals the actual and practical performances of different receivers exposed to time-varying channels with respect to the ideal scenario.

5.7 Summary

In this chapter, we have employed a realistic approach to estimate the time-varying channel coefficients by PSAM. With these estimates, we can then assess the BER of different reception methods (ML. CML, AR, ZF and DF) by simulations. Our results have shown that all detection methods, except CML detection, achieve nearly the same BER performance over time-varying channels. In many cases, CML detection performs the best by about 5dB due to the diversity gain. However, their BER performances degrade when the channels vary very fast. Besides, under the ideal situations that perfect channel state information is available at the receiver, we have derived closed-form expressions of ZF and DF detections and discuss the discrepancies in terms of BER among all receivers. Our results have shown that in general, CML detection is the best reception scheme among all due to third order diversity, with the help of separated signal transmissions. The first runner-up is ML. DF comes next and it is slightly better than ZF. And the worst one is AR.

And, the influence of time-varying channels results in the error flooring effect. In accordance with our numerical results, we can conclude that if we cannot have good channel estimates, with PSAM, we cannot get any benefit by using ML or a diversity gain by using CML that can obtain better performance yet, at the expense of the reception complexity.

□ **End of chapter.**

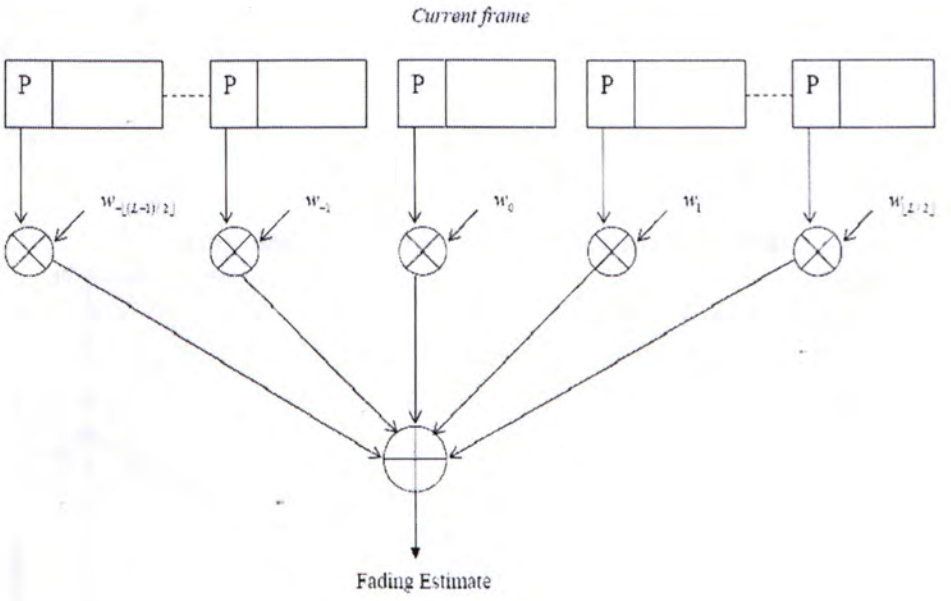

Figure 5.1: Fading interpolation in PSAM.

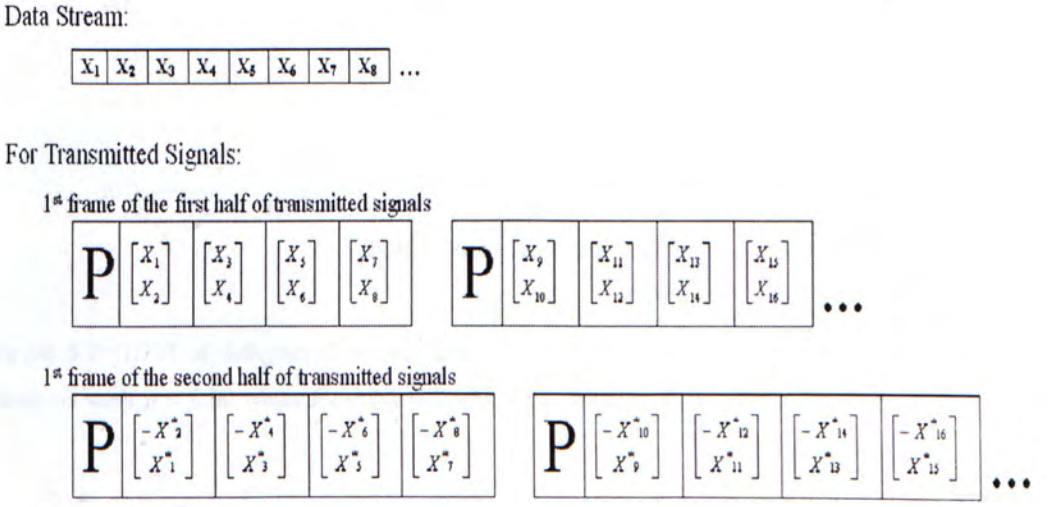

Figure 5.2: A diagram showing how to transmit the signals so as to decrease the dependency of the channels.

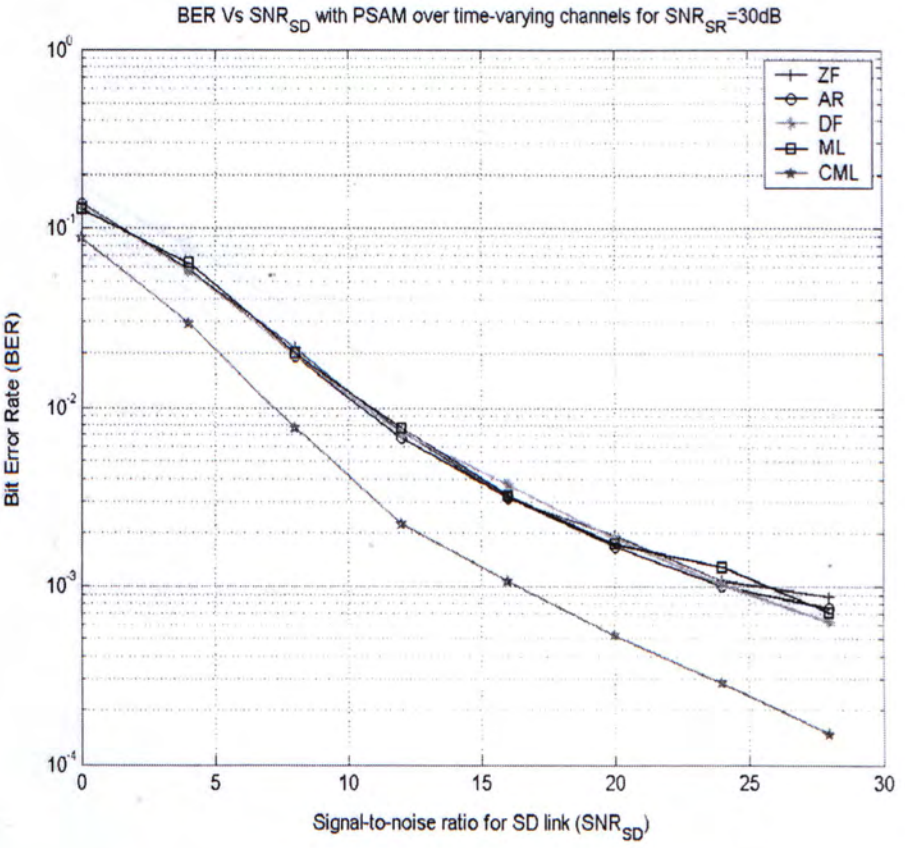

Figure 5.3: BER of different detectors with PSAM for fading $R \rightarrow D$ link over time-varying channels with $\rho = 0.99$ when $E_{SR}/N_0 = 30$dB, $M = 7$ and $L = 5$.

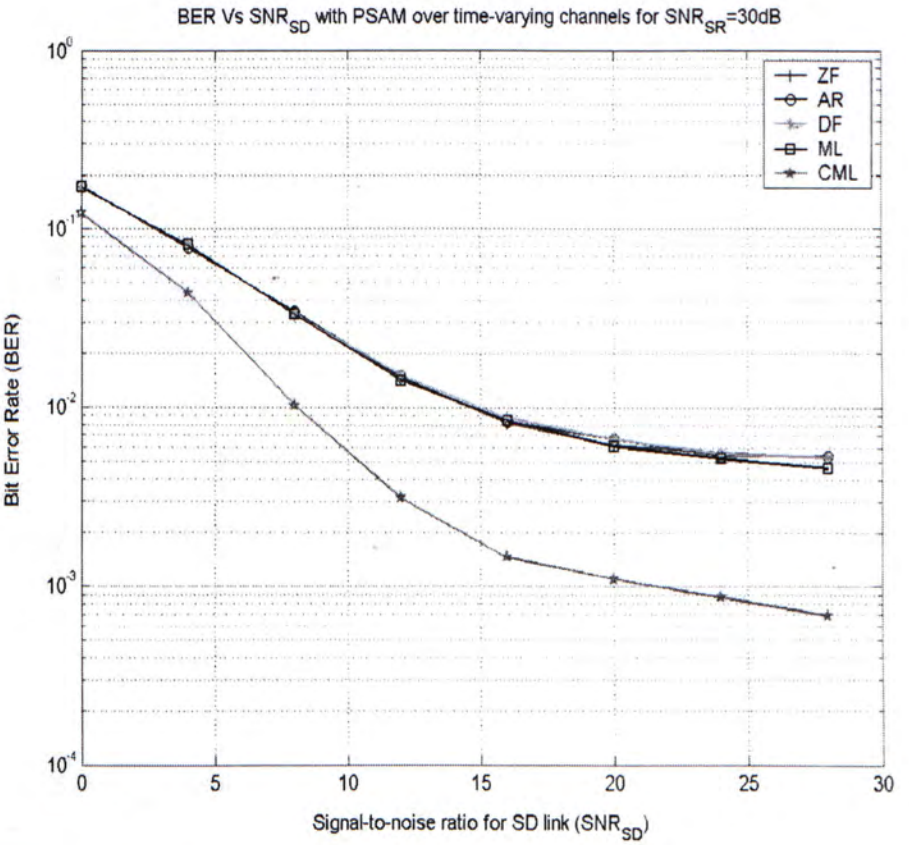

Figure 5.4: BER of different detectors with PSAM for fading $R \rightarrow D$ link over time-varying channels with $\rho = 0.9755$ when $E_{SR}/N_0 = 30$dB, $M = 7$ and $L = 5$.

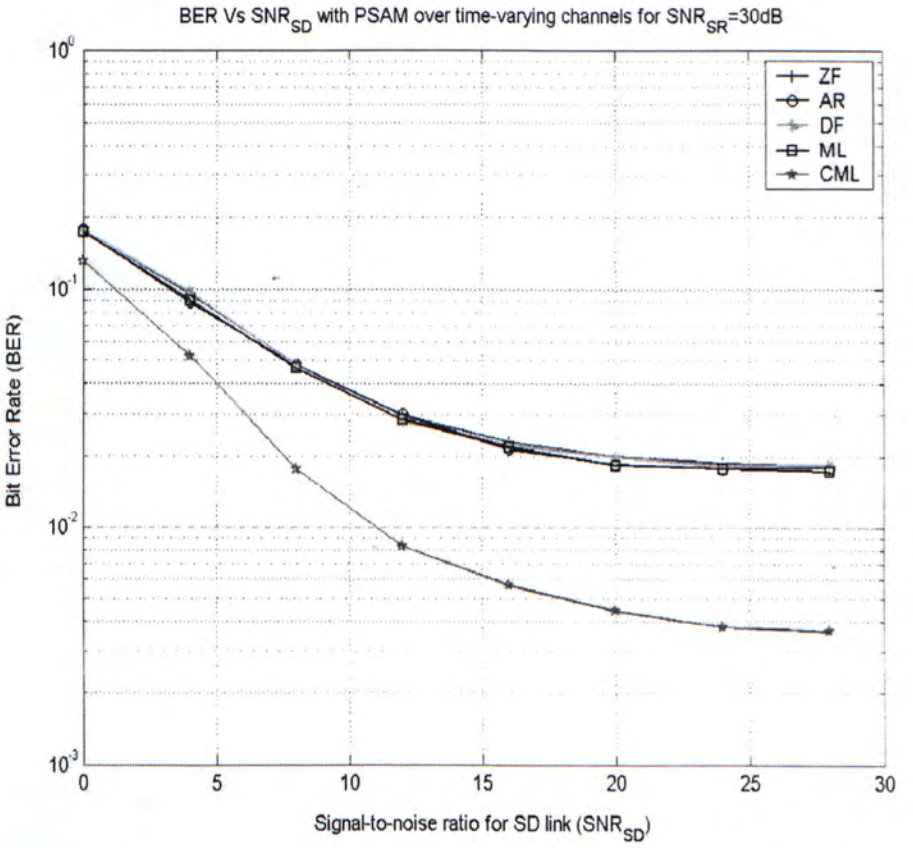

Figure 5.5: BER of different detectors with PSAM for fading $R \rightarrow D$ link over time-varying channels with $\rho = 0.95$ when $E_{SR}/N_0 = 30$dB, $M = 7$ and $L = 5$.

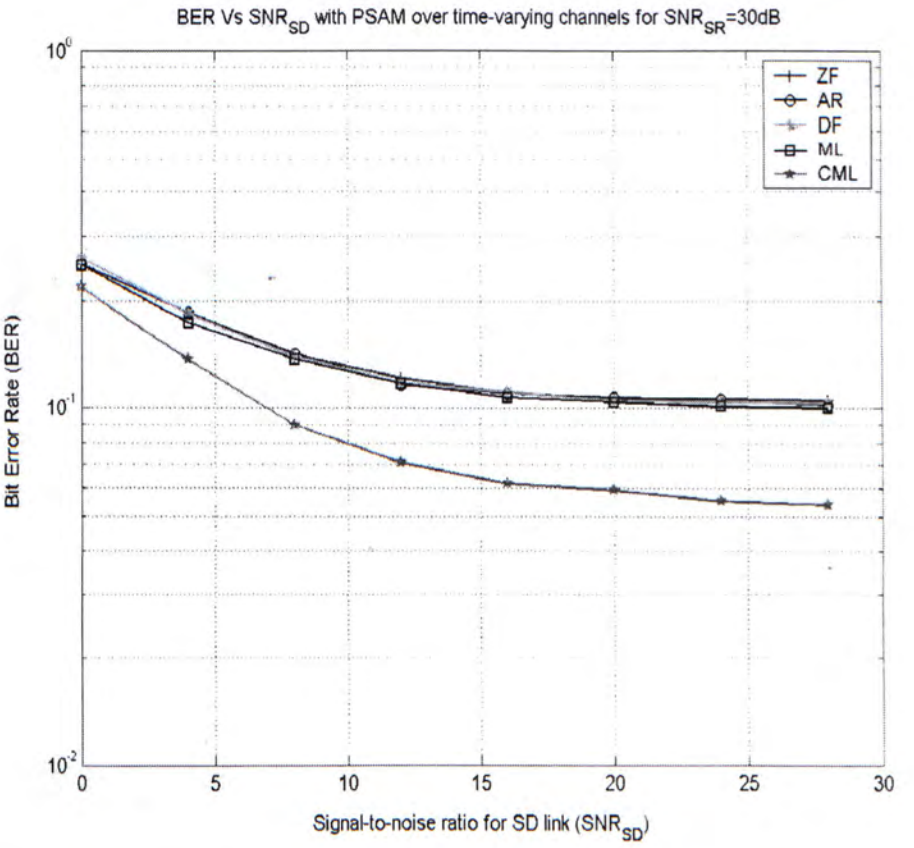

Figure 5.6: BER of different detectors with PSAM for fading $R \rightarrow D$ link over time-varying channels with $\rho = 0.9037$ when $E_{SR}/N_0 = 30$dB, $M = 7$ and $L = 5$.

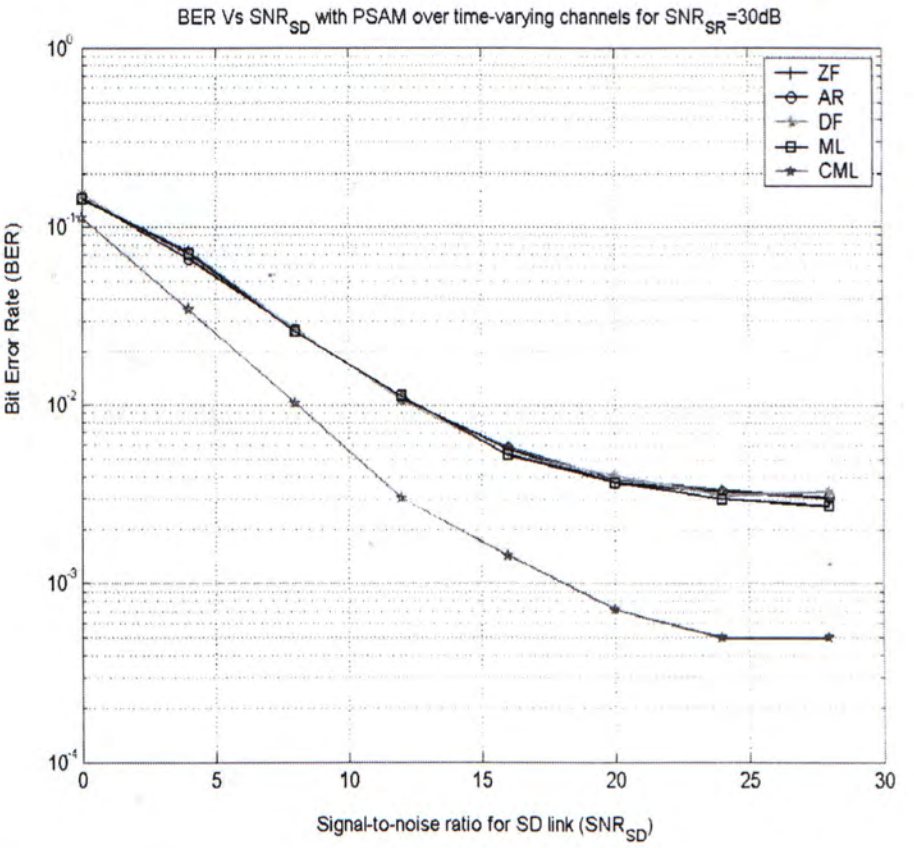

Figure 5.7: BER of different detectors with PSAM for fading $R \rightarrow D$ link over time-varying channels with $\rho = 0.9755$ when $E_{SR}/N_0 = 30$dB, $M = 5$ and $L = 5$.

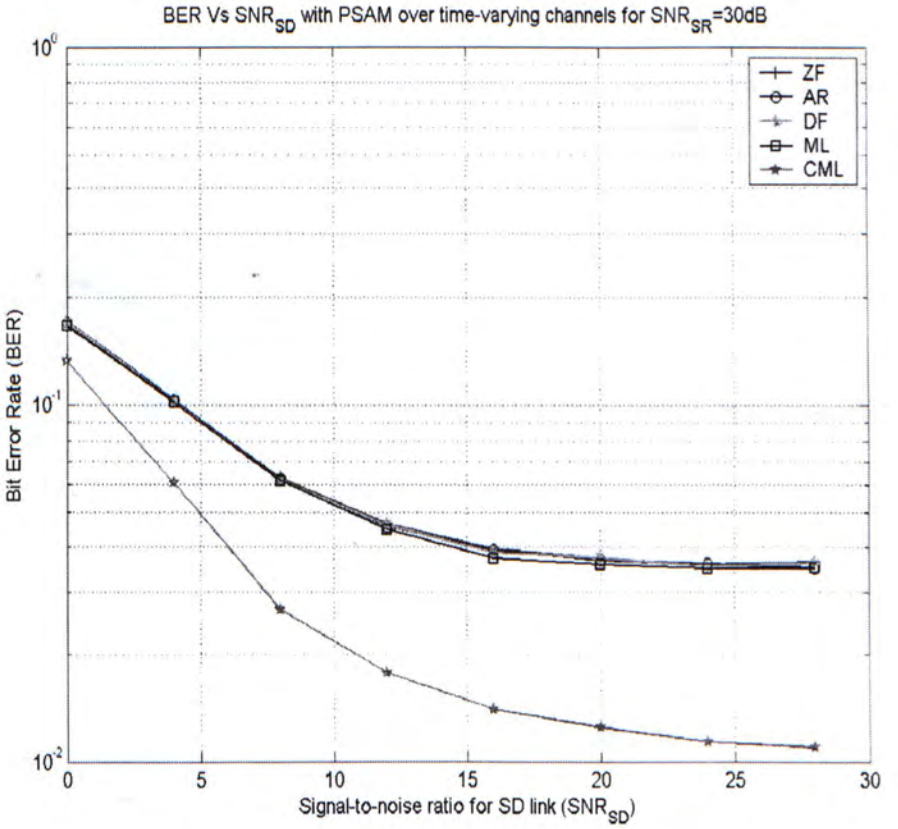

Figure 5.8: BER of different detectors with PSAM for fading $R \rightarrow D$ link over time-varying channels with $\rho = 0.9037$ when $E_{SR}/N_0 = 30$dB, $M = 5$ and $L = 5$.

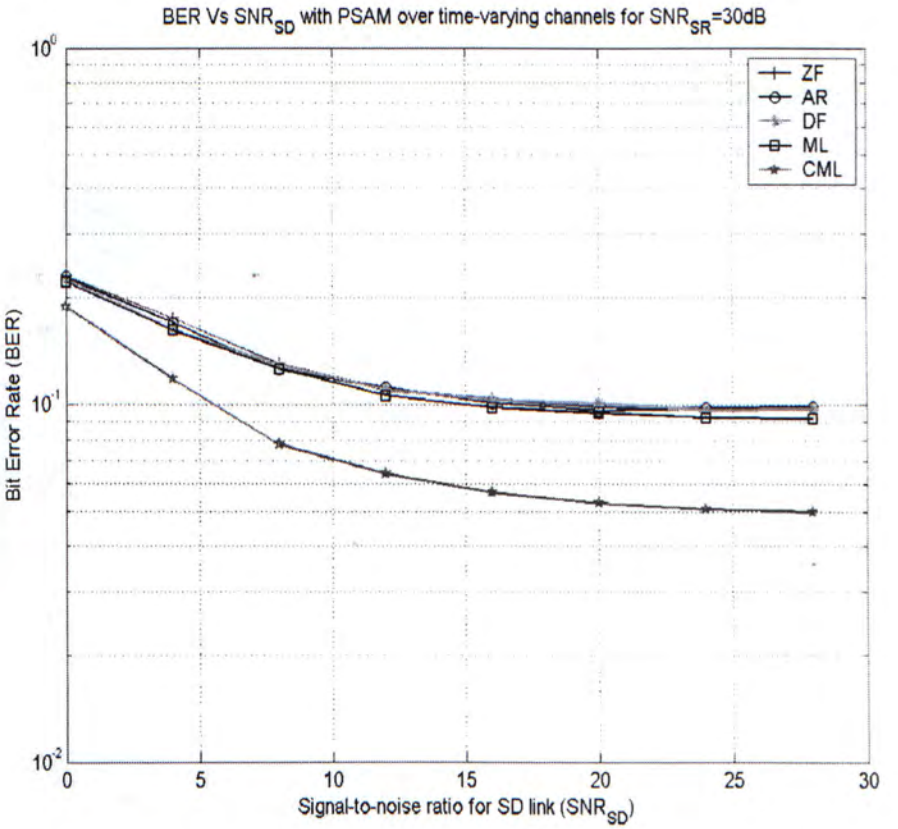

Figure 5.9: BER of different detectors with PSAM for fading $R \rightarrow D$ link over time-varying channels with $\rho = 0.85$ when $E_{SR}/N_0 = 30$dB, $M = 5$ and $L = 5$.

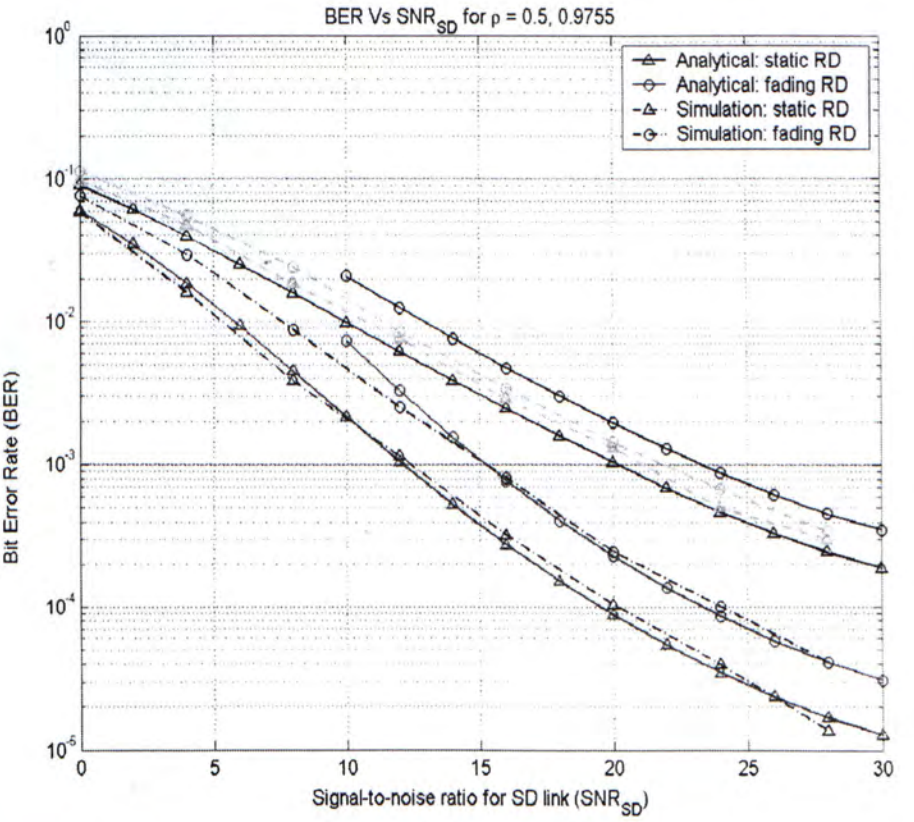

Figure 5.10: Comparison of simulation results and our analytical results for DF. Upper curves: $\rho = 0.5$; Lower curves: $\rho = 0.9755$.

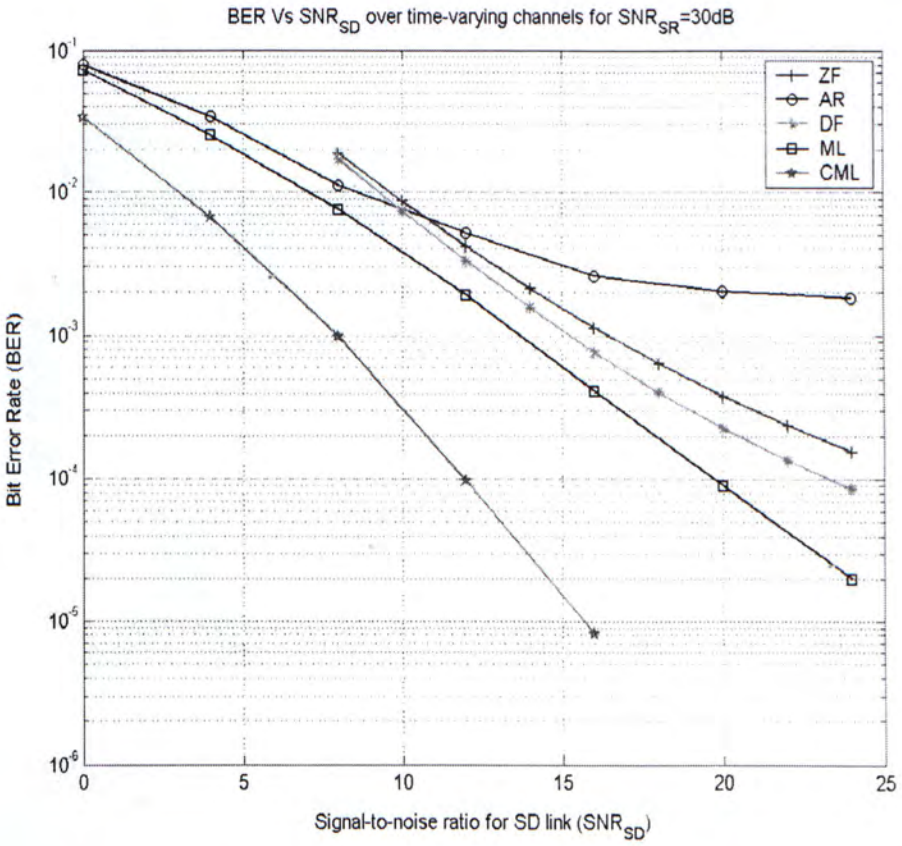

Figure 5.11: BER of different detectors with perfect channel state information for fading $R \rightarrow D$ link over time-varying channels with $\rho = 0.9755$ when $E_{SR}/N_0 = 30$dB.

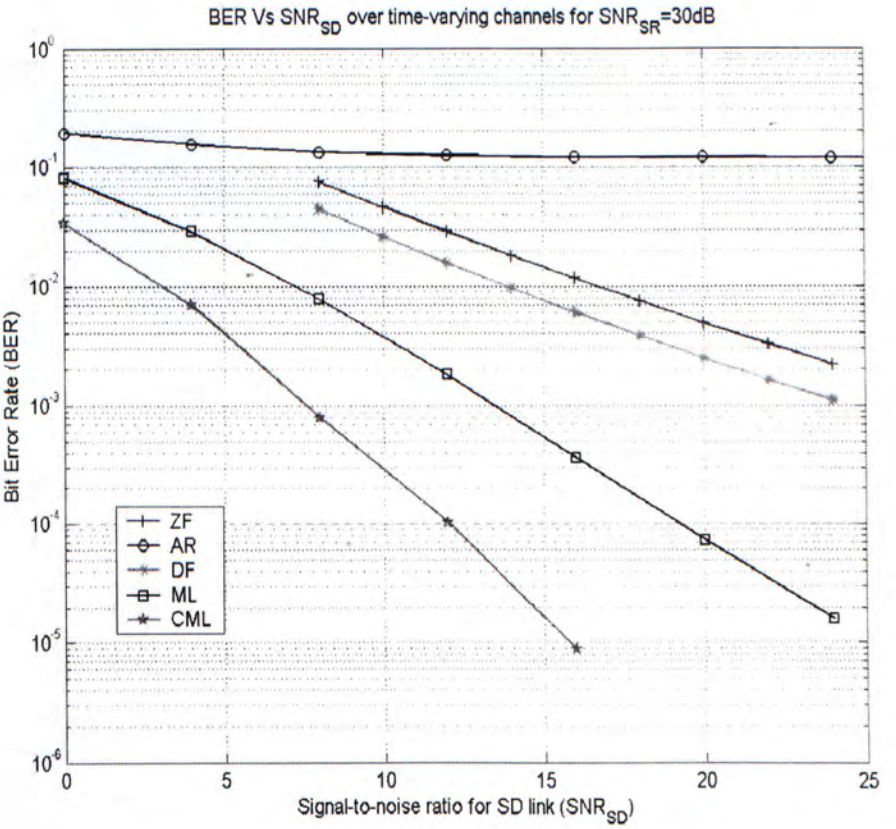

Figure 5.12: BER of different detectors with perfect channel state information for fading $R \rightarrow D$ link over time-varying channels with $\rho = 0.5$ when $E_{SR}/N_0 = 30$dB.

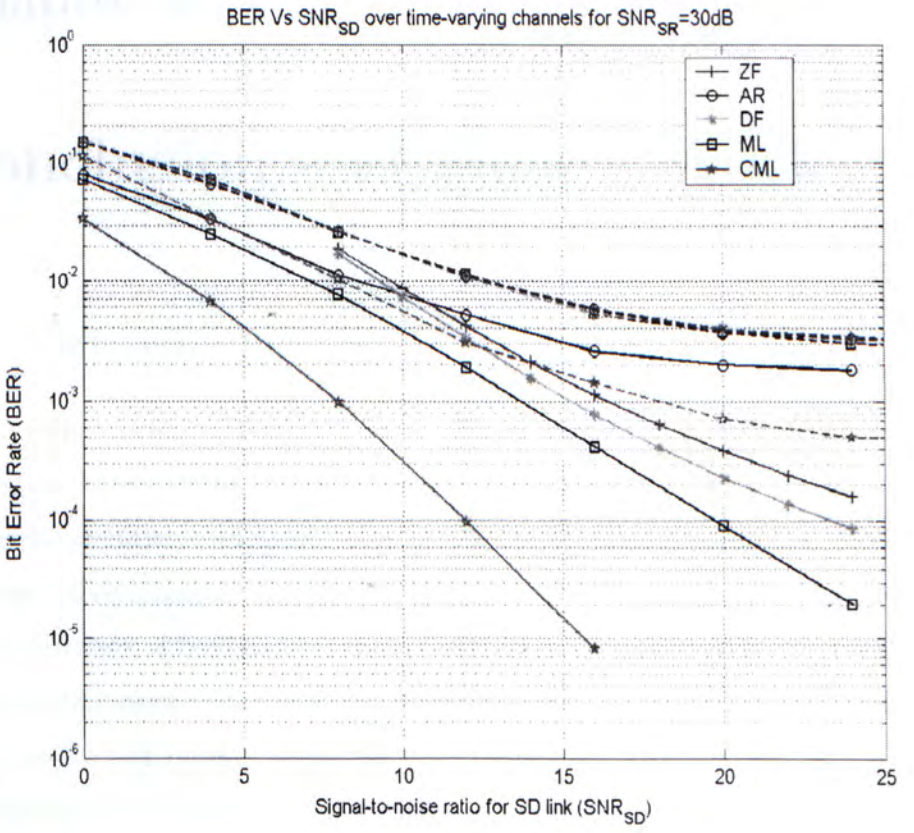

Figure 5.13: Comparison of the BER performances of different reception schemes with PSAM and that with perfect channel state information for fading $R \rightarrow D$ link over time-varying channels with $\rho = 0.9755$ when $E_{SR}/N_0 = 30$dB. Dotted curves: PSAM; Solid curves: Perfect Channel State Information.

Chapter 6

Conclusion and Future Work

6.1 Conclusion

To sum up, in this thesis, we have studied a number of issues of the distributed space-time block coding in user cooperative communications. Undeniably, the topic of user cooperative communications in wireless systems is emerging. In chapter 3, through closely investigating the 3-node system model, we have analyzed its performance in terms of the bit-error-rate (BER) by deriving closed-form expressions for a distributed space-time block coded system under perfect channel estimation and time-invariant channels. With the distributed Alamouti's space-time block code and appropriate power control, we have shown that the maximum diversity order is obtained. Besides, we have discussed the appearance of the error floor and how to avoid this, thereby allowing reliable communications in cooperative networks.

Next, in chapter 4, we have considered the facet of imperfect channel estimation. Our results have indicated that the effect of imperfect channel estimation manifests itself as an error floor. With suitable power control, our analytical BER results perfectly match with simulation results. We have found that, for $E_{SD} = E_{RD}$, the lowest error floor and the optimal performance for imperfect channel estimation can

be achieved. Under acceptable power imbalance, our analytical expressions provide tight bounds to simulation results.

In addition, in chapter 5, we have further studied the performance over time-varying channels. We have analyzed the performances with different reception schemes, namely maximum likelihood in [29] and cooperative maximum likelihood, Alamouti's receiver, zero-forcing and decision-feedback. First, we have exploited PSAM to estimate the time-varying channel coefficients for assessing the BER by simulations. With PSAM, all receivers, except CML receiver, achieve similar performance over time-varying channels. Withe the help of separated signal transmission, ascribed to the diversity gain, cooperative maximum likelihood detection performs the best and prevails over the others by about 5dB. Second, assuming that the exact channel coefficients are available at the receiver, we have derived closed-form expressions of reception methods of zero-forcing and decision-feedback. Our results have shown that the cooperative maximum likelihood detection and maximum likelihood detection in [29] outperform the others, followed by decision-feedback receiver and zero-forcing receiver. The worst one is Alamouti's receiver. In particular, cooperative maximum likelihood detection is the best because of the third order diversity. On the whole, the effect of time-varying channels induces an error floor.

In short, user cooperative communications are attractive and to be successfully used in wireless networks, e.g. ad hoc networks. In such an ambience that does not have a fixed network topology and infrastructure, distributed space-time block coding based cooperation indeed helps reduce the probability of error, thereby guaranteeing reliable communication channels and robustness to channel variations.

6.2 Future Work

There are loads of work we can proceed in this area. Chief among them is the design and analysis of generalized cooperative networks. In this topic, there are some aspects we can further study, including design of code matrix and adaptive protocols.

6.2.1 Design of Code Matrix

In multi-source cooperation, the design of code matrix is crucial in order to minimize the error probability. For example, by assuming the simultaneous transmission is not allowed, if the number of sources is four, and the desired order of diversity is three and the desired data rate is 0.5 symbol per time, the following code matrix can fulfill the requirement:

$$\begin{bmatrix} x_1 & 0 & 0 & 0 \\ 0 & x_2 & 0 & 0 \\ 0 & 0 & x_3 & 0 \\ 0 & 0 & 0 & x_4 \\ x_2 \bigoplus x_3 & 0 & 0 & 0 \\ 0 & x_3 \bigoplus x_4 & 0 & 0 \\ 0 & 0 & x_4 \bigoplus x_1 & 0 \\ 0 & 0 & 0 & x_1 \bigoplus x_2 \end{bmatrix}, \tag{6.1}$$

where $\bigoplus$ is an exclusive OR operation.

Another proposal is to make use of Reed-Solomon (RS) codes [19]. This cooperation consists of two phases. In the first phase, each node transmits its own information or symbol to the destination. Meanwhile, each node decodes these

transmissions and applied a RS encoder to the decoded data. In the second phase, each node transmits its RS code to the destination. This scheme can be shown to achieve D^{th} order diversity ($0 < D \leq N$) with a code rate up to $1-(D-1)/N$ [24], where N is the number of nodes in the network. The key advantage of this cooperation mechanism is that the degree of diversity and the rate can be adjusted in accordance with the use of RS codes. Nonetheless, transmission with full diversity and full rate is not possible. In order to achieve maximum diversity order with full rate, rotation of signal constellations may help [25], for instance, for four transmit antennas, the quasi-orthogonal space-time block codes with full diversity is given by

$$C = \begin{bmatrix} x_1 & x_2 & x_3 & x_4 \\ -x_2^* & x_1^* & -x_4^* & x_3^* \\ x_3 & x_4 & x_1 & x_2 \\ -x_3^* & x_4^* & -x_2^* & x_1^* \end{bmatrix}, \tag{6.2}$$

where $x_1, x_2 \in \mathcal{A}$ and $x_3, x_4 \in e^{j\phi}\mathcal{A}$ for some signal constellation $\mathcal{A}$, and the rotation angle ϕ is determined by the signal constellation $\mathcal{A}$. With appropriate rotation angle, for example $\phi = \pi/4$ for QAM, the code matrix C is a full rank matrix, meaning that maximum diversity can be achieved with full rate. Thus far, how we can design an optimal transmission scheme remains an open problem.

6.2.2 Adaptive Protocols

Some research studies have shown that the position of relay is an important factor [20, 21]. In a simple signal forwarding scheme, to achieve the optimal performance, the relay should be located just in the middle between the source and the destination [21]. For some Direct Sequence Code Division Multiple Access (DS-CDMA) schemes, the relay or cooperating terminal should be placed as close as possible

to the source [20]. Yet, it is still passive with respect to the position of relay(s). The idea of adaptive protocols is that no matter how the relays are placed, we still achieve the optimal performance by adopting adaptive cooperative protocols, which are not yet to be found.

The foregoing topics are not only fascinating and challenging, but also useful and practical. We hope that these conceptual ideas will be implemented in practice and contribute to our community.

□ **End of chapter.**

Appendix A

Derivation of (3.23)

From (3.20),

$$D = \sum_{k=1}^{L} \left(A|X_k|^2 + B|Y_k|^2 + CX_kY_k^* + C^*X_k^*Y_k \right) \tag{A.1}$$

consists of complex-valued Gaussian random variable [17]. A, B and C are constants; X_k and Y_k are a pair of correlated complex-Gaussian random variables and the L pairs of X_k, Y_k are mutually statistically independent. The probability of error is the probability that $D < 0$, which can be evaluated by the characteristic function, denoted by $\psi_D(j\upsilon)$ of the general quadratic form. The probability that $D < 0$, denoted by $P(e)$ is

$$P(e) = P(D < 0) = \int_{-\infty}^{0} p(D)dD \tag{A.2}$$

where $p(D)$, the probability density function of D, is related to $\psi_D(j\upsilon)$ by the Fourier Transform, i.e.,

$$p(D) = \frac{1}{2\pi} \int_{-\infty}^{\infty} \psi_D(j\upsilon) e^{-j\upsilon D} d\upsilon. \tag{A.3}$$

Hence,

$$P(e) = \int_{-\infty}^{0} dD \frac{1}{2\pi} \int_{-\infty}^{\infty} \psi_D(j\upsilon) e^{-j\upsilon D} d\upsilon. \tag{A.4}$$

Let interchange the order of integration and integrate with respect to D first. The expression becomes

$$P(e) = -\frac{1}{2\pi j}\int_{\infty-j\epsilon}^{\infty+j\epsilon}\frac{\psi_D(j\upsilon)}{\upsilon}d\upsilon, \tag{A.5}$$

where a small positive number ϵ has been inserted in order to move the path of integration away from zero. Since D is the sum of statistically independent random variables, the characteristic function of D factors into a product of L characteristic functions, with each function corresponding to the individual random variables d_k shown in (3.21) and its characteristic function is

$$\psi_{d_k}(j\upsilon) = \frac{\upsilon_{1k}\upsilon_{2k}}{(\upsilon+j\upsilon_{1k})(\upsilon-j\upsilon_{2k})}\exp\left[\frac{\upsilon_{1k}\upsilon_{2k}\left(-\upsilon^2\lambda_{1k}+j\upsilon\lambda_{2k}\right)}{(\upsilon+j\upsilon_{1k})(\upsilon-j\upsilon_{2k})}\right] \tag{A.6}$$

where

$$\upsilon_{1k} = \sqrt{m_k^2+\frac{1}{4\left(\mu_{x_kx_k}\mu_{y_ky_k}-|\mu_{x_ky_k}|^2\right)\left(|C|^2-AB\right)}}-m_k \tag{A.7}$$

$$\upsilon_{1k} = \sqrt{m_k^2+\frac{1}{4\left(\mu_{x_kx_k}\mu_{y_ky_k}-|\mu_{x_ky_k}|^2\right)\left(|C|^2-AB\right)}}+m_k \tag{A.8}$$

$$m_k = \frac{A\mu_{x_kx_k}+B\mu_{y_ky_k}+C\mu^*_{x_ky_k}+C^*\mu_{x_ky_k}}{4\left(\mu_{x_kx_k}\mu_{y_ky_k}-|\mu_{x_ky_k}|^2\right)\left(|C|^2-AB\right)} \tag{A.9}$$

$$\mu_{x_ky_k} = \frac{1}{2}E\left[\left(X_k-\bar{X}_k\right)\left(Y_k-\bar{Y}_k\right)\right] \tag{A.10}$$

and as $\bar{X}_k = \bar{Y}_k = 0$,

$$\lambda_{1k} = 0 \tag{A.11}$$

$$\lambda_{2k} = 0. \tag{A.12}$$

Thus,

$$\psi_{d_1}(j\upsilon) = \frac{\upsilon_{11}\upsilon_{21}}{(\upsilon+j\upsilon_{11})(\upsilon-j\upsilon_{21})} \tag{A.13}$$

$$\psi_{d_2}(j\upsilon) = \frac{\upsilon_{12}\upsilon_{22}}{(\upsilon+j\upsilon_{12})(\upsilon-j\upsilon_{22})}. \tag{A.14}$$

Due to the independence of the random variables d_k, the characteristic function of D is

$$\psi_D(jv) = \psi_{d_1}(jv)\psi_{d_2}(jv) \tag{A.15}$$

$$= \frac{v_{11}v_{21}}{(v+jv_{11})(v-jv_{21})}\frac{v_{12}v_{22}}{(v+jv_{12})(v-jv_{22})} \tag{A.16}$$

and the error probability, given $|h_{RD}|$,

$$P(e) = -\frac{1}{2\pi j}\int_{\infty-j\epsilon}^{\infty+j\epsilon}\frac{\psi_D(jv)}{v}dv \tag{A.17}$$

$$= -\frac{v_{11}v_{21}v_{12}v_{22}}{2\pi j}\int_{\infty-j\epsilon}^{\infty+j\epsilon}\frac{dv}{v(v+jv_{11})(v-jv_{21})(v+jv_{12})(v-jv_{22})}. \tag{A.18}$$

By using contour integration, we have

$$\begin{aligned}\int_C f(z)dz &= \int_{-R+j\epsilon}^{R+j\epsilon}\frac{dv}{v(v+jv_{11})(v-jv_{21})(v+jv_{12})(v-jv_{22})} \\ &\quad + \int_\gamma \frac{dz}{z(z+jv_{11})(z-jv_{21})(z+jv_{12})(z-jv_{22})} \\ &= 2\pi j\sum\{\text{ Residues of } f(z) \text{ inside the closed contour }\}. \end{aligned} \tag{A.19}$$

As v_{11}, v_{12}, v_{21} and v_{22} are positive, $f(z)$ has simple poles only at jv_{21} and jv_{22} inside C.

Consider

$$\begin{aligned} &Res_{z=jv_{21}}f(z) \\ &= \lim_{z\to jv_{21}}\left[(z-jv_{21})\frac{1}{z(z+jv_{11})(z-jv_{21})(z+jv_{12})(z-jv_{22})}\right] \\ &= \frac{1}{v_{21}(v_{21}+v_{11})(v_{21}+v_{12})(v_{21}-v_{22})} \end{aligned} \tag{A.20}$$

and

$$\begin{aligned} &Res_{z=jv_{22}}f(z) \\ &= \lim_{z\to jv_{22}}\left[(z-jv_{22})\frac{1}{z(z+jv_{11})(z-jv_{21})(z+jv_{12})(z-jv_{22})}\right] \\ &= \frac{1}{v_{22}(v_{22}+v_{11})(v_{22}-v_{21})(v_{22}+v_{12})}, \end{aligned} \tag{A.21}$$

now, on γ, $z = Re^{j\theta}$, the second term in (A.19) will vanish when R tends to infinity. As in our case, $\Upsilon_1 = \sum_{k=1}^{2} Re\{X_k Y_k^*\}$, $A = B = 0$ and $C = C^* = 1/2$. Thus, (A.17) becomes

$$P(e) = -\frac{\upsilon_{11}\upsilon_{21}\upsilon_{12}\upsilon_{22}}{2\pi j}\left[2\pi j\left(Res_{z=j\upsilon_{21}} f(z) + Res_{z=j\upsilon_{22}} f(z)\right)\right] \tag{A.22}$$

By substitution, (3.23) is obtained:

$$P(e) = \frac{-\upsilon_{11}\upsilon_{12}\upsilon_{22}}{(\upsilon_{21}+\upsilon_{11})(\upsilon_{21}+\upsilon_{12})(\upsilon_{21}-\upsilon_{22})} + \frac{-\upsilon_{11}\upsilon_{12}\upsilon_{21}}{(\upsilon_{22}+\upsilon_{21})(\upsilon_{22}-\upsilon_{21})(\upsilon_{22}+\upsilon_{12})} \tag{A.23}$$

where

$$\upsilon_{11} = \sqrt{\frac{4}{N_0^2} + \frac{1}{\frac{1}{4}\left(\frac{E_{SR}E_{RD}}{1+E_{SR}/N_0+E_{RD}/N_0}\right)|h_{RD}|^2}} - \frac{2}{N_0} \tag{A.24}$$

$$\upsilon_{12} = \sqrt{\frac{4}{N_0^2} + \frac{1}{\frac{1}{4}\left(\frac{E_{SR}E_{RD}}{1+E_{SR}/N_0+E_{RD}/N_0}\right)|h_{RD}|^2}} + \frac{2}{N_0} \tag{A.25}$$

$$\upsilon_{21} = \sqrt{\frac{4}{N_0^2} + \frac{1}{\frac{1}{4}\left(\frac{(E_{SR}+N_0)E_{SD}}{1+E_{SR}/N_0+E_{RD}/N_0}\right)}} - \frac{2}{N_0} \tag{A.26}$$

$$\upsilon_{22} = \sqrt{\frac{4}{N_0^2} + \frac{1}{\frac{1}{4}\left(\frac{(E_{SR}+N_0)E_{SD}}{1+E_{SR}/N_0+E_{RD}/N_0}\right)}} + \frac{2}{N_0}. \tag{A.27}$$

□ **End of chapter.**

Appendix B

Derivation of (3.30) and (3.32)

The received signals are given by (3.5) and (3.6). The decision statistics are constructed as

$$\begin{aligned}\tilde{x_1} &= \alpha h_1^* r_1 + \beta h_2 r_2^* \\ &= \left(\alpha^2|h_1|^2 + \beta^2|h_2|^2\right) x_1 + \alpha h_1^* n_1 + \beta h_2 n_2^*, \qquad \text{(B.1)} \\ \tilde{x_2} &= \beta h_2^* r_1 - \alpha h_1 r_2^* \\ &= \left(\alpha^2|h_1|^2 + \beta^2|h_2|^2\right) x_2 - \alpha h_1 n_2^* + \beta h_2^* n_1. \qquad \text{(B.2)}\end{aligned}$$

Here, h_1 and h_2 are complex Gaussian random variables with zero mean and unit variance, i.e. $h_i = |h_i|e^{j\theta_i}$ for $i = 1, 2$, where $|h_i|$ is Rayleigh distributed and θ_i is uniform distributed. Due to the symmetry of the problem, we only focus on $\tilde{x_1}$ afterwards. Normalizing $\tilde{x_1}$, we define

$$\hat{x_1} = \frac{\tilde{x_1}}{\alpha^2|h_1|^2 + \beta^2|h_2|^2} = x_1 + \frac{\alpha h_1^* n_1 + \beta h_2 n_2^*}{\alpha^2|h_1|^2 + \beta^2|h_2|^2}. \qquad \text{(B.3)}$$

Now, we introduce the error term

$$\begin{aligned}\xi &= \hat{x_1} - x_1 \qquad \text{(B.4)} \\ &= \frac{\alpha|h_1|}{\alpha^2|h_1|^2 + \beta^2|h_2|^2}\tilde{n_1} + \frac{\beta|h_2|}{\alpha^2|h_1|^2 + \beta^2|h_2|^2}\tilde{n_2} \qquad \text{(B.5)}\end{aligned}$$

where we define

$$\tilde{n_1} = e^{-j\theta_1} n_1 = \tilde{n}_{1R} + j\tilde{n}_{1I}, \tag{B.6}$$

$$\tilde{n_2} = e^{j\theta_2} n_2^* = \tilde{n}_{2R} + j\tilde{n}_{2I}, \tag{B.7}$$

where $\tilde{n}_{iR}$ and $\tilde{n}_{iI}$ are zero-mean complex Gaussian random variables with variance N_0 , i.e. $\tilde{n}_{iR}$, $\tilde{n}_{iI} \sim N(0, N_0)$, for $i = 1, 2$. Conditioned on $|h_1|$ and $|h_2|$, $\xi = \xi_R + j\xi_I$ is complex Gaussian, i.e.

$$\xi_R, \xi_I \sim N\left(0, \frac{N_0}{\alpha^2|h_1|^2 + \beta^2|h_2|^2}\right). \tag{B.8}$$

Joint pdf of ξ_R and ξ_I is given as

$$f(\xi_R, \xi_I||h_1|, |h_2|) = \frac{1}{2\pi\sigma_\xi^2} \exp\left(-\frac{1}{2\sigma_\xi^2}(\xi_R^2 + \xi_I^2)\right). \tag{B.9}$$

Performing expectations with respect to $|h_i|$ which follows a Rayleigh distribution,

$$f(|h_i|) = \frac{|h_i|}{\sigma_{h_i}^2} \exp\left(-\frac{|h_i|^2}{2\sigma_{h_i}^2}\right), \text{ for } i = 1, 2, \tag{B.10}$$

where $E[|h_i|^2] = 2\sigma_{h_i}^2$, we obtain

$$f(\xi_R, \xi_I) = \frac{\varphi_1}{\pi} \frac{1}{(w_1 + \varphi_1\xi_I^2)^2(w_2 + \varphi_2\xi_I^2)} + \frac{\varphi_2}{\pi} \frac{1}{(w_1 + \varphi_1\xi_I^2)(w_2 + \varphi_2\xi_I^2)^2}. \tag{B.11}$$

Here, $w_i = 1 + \varphi_i\xi_R^2$, $\varphi_i = \bar{E}_i/2\sigma_n^2$ and $E_1 = \alpha^2$, $E_2 = \beta^2$ with their averages $\bar{E}_i = E_i \cdot (2\sigma_{h_i}^2)$. Define d to be the half of the separation between the constellation points x_1 and x_2 of BPSK modulation. BER is obtained by performing the two-dimensional integration

$$P(e) = \int_{\xi_R=d}^{\infty} \left[\int_{\xi_I=-\infty}^{\infty} f(\xi_R, \xi_I) d\xi_I\right] d\xi_R \tag{B.12}$$

which yields (3.30) for $\bar{\gamma}_1 \neq \bar{\gamma}_2$ and (3.32) for $\bar{\gamma}_1 = \bar{\gamma}_2 = \bar{\gamma}$.

□ **End of chapter.**

Appendix C

Derivation of (4.9) and (4.13)

Starting from (4.5), due to symmetry, we focus merely on $\tilde{x_1}$ and we can write $\tilde{x_1}$ as

$$\begin{aligned}\tilde{x_1} = &\left(\alpha\rho|\hat{h}_1|^2 + \beta\rho|\hat{h}_2|^2\right)x_1 + \left(\alpha\hat{h}_1^* d_1 + \beta\hat{h}_2 d_2\right)x_1 \\ &+ \left(\beta\hat{h}_1^* d_2 - \alpha\hat{h}_2 d_1^*\right)x_2 + \hat{h}_1^* n_1 + \hat{h}_2 n_2^* + \rho\hat{h}_1^*\hat{h}_2(\beta-\alpha)x_2. \end{aligned} \tag{C.1}$$

For BPSK modulation, BER is given as

$$\begin{aligned}P(e|x_1, |\hat{h}_1|, |\hat{h}_2|) = &P(x_1 = 1)P(e|x_1 = 1, |\hat{h}_1|, |\hat{h}_2|) \\ &+ P(x_1 = -1)P(e|x_1 = -1, |\hat{h}_1|, |\hat{h}_2|). \end{aligned} \tag{C.2}$$

Assuming $E_{SR}/N_0 \gg 1$, and noting $\beta/\alpha = \sqrt{n}$, by ignoring the last term, we have

$$P(e||\hat{h}_1|, |\hat{h}_2|) = Q\left(\sqrt{\frac{\rho^2\beta^2}{(1+n)\alpha^2\sigma_d^2 + \sigma_n^2}\frac{(\frac{1}{\sqrt{n}}|\hat{h}_1|^2 + |\hat{h}_2|^2)^2}{(|\hat{h}_1|^2 + |\hat{h}_2|^2)}}\right) \tag{C.3}$$

which can be approximated as

$$P(e||\hat{h}_1|, |\hat{h}_2|) \approx Q\left(\sqrt{\frac{\rho^2\beta^2}{(1+n)\alpha^2\sigma_d^2 + \sigma_n^2}(\frac{1}{\sqrt{n}}|\hat{h}_1|^2 + |\hat{h}_2|^2)}\right). \tag{C.4}$$

Denote,

$$\varepsilon_1 = \frac{1}{\sqrt{n}} \frac{\rho^2\beta^2}{(1+n)\alpha^2\sigma_d^2 + \sigma_n^2} |\hat{h}_1|^2, \tag{C.5}$$

$$\varepsilon_2 = \frac{\rho^2\beta^2}{(1+n)\alpha^2\sigma_d^2 + \sigma_n^2} |\hat{h}_2|^2 \tag{C.6}$$

where ε_1 and ε_2 are independent and exponentially distributed, i.e. $f_{\varepsilon_i}(\varepsilon_i) = 1/\bar{\varepsilon_i} \exp(-\varepsilon_i/\bar{\varepsilon_i})$. As $\hat{h}_i = h_i + z_i$, then $\sigma^2_{\hat{h}_i} = \sigma^2_{h_i} + \sigma^2_{z_i}$. For non-fading $R \to D$ link, $h_{RD} = 1$ we have,

$$\bar{\varepsilon_1} = \frac{1}{\sqrt{n}} \frac{2\beta^2 \cdot \Gamma}{(1+n)\alpha^2 \cdot \nu \cdot \Gamma + 1 + \nu}, \tag{C.7}$$

$$\bar{\varepsilon_2} = \frac{2\beta^2 \cdot \Gamma}{(1+n)\alpha^2 \cdot \nu \cdot \Gamma + 1 + \nu} \tag{C.8}$$

where $\nu = \sigma_z^2/\sigma_h^2$ and $\Gamma = \sigma_h^2/\sigma_n^2$. Therefore, the BER expression is given by

$$\begin{aligned} P(e) &= \int_0^\infty \int_0^\infty P(e||\hat{h}_1|, |\hat{h}_2|) f_{\varepsilon_1}(\varepsilon_1) f_{\varepsilon_2}(\varepsilon_2) d\varepsilon_1 d\varepsilon_2 \\ &\approx \int_0^\infty \int_0^\infty Q(\sqrt{\varepsilon_1 + \varepsilon_2}) f_{\varepsilon_1}(\varepsilon_1) f_{\varepsilon_2}(\varepsilon_2) d\varepsilon_1 d\varepsilon_2. \end{aligned} \tag{C.9}$$

Introducing the "alternative" definition for Q(.) function [5],

$$P(e) \approx \int_0^\infty \int_0^\infty \frac{1}{\pi} \int_0^{\pi/2} e^{-\frac{\varepsilon_1+\varepsilon_2}{2\sin^2\theta}} d\theta f_{\varepsilon_1}(\varepsilon_1) f_{\varepsilon_2}(\varepsilon_2) d\varepsilon_1 d\varepsilon_2 \tag{C.10}$$

$$= \frac{1}{\pi} \int_0^{\pi/2} \left(\frac{\sin^2\theta}{\sin^2\theta + \bar{\varepsilon_1}/2} \right) \left(\frac{\sin^2\theta}{\sin^2\theta + \bar{\varepsilon_2}/2} \right) d\theta. \tag{C.11}$$

For $E_{SR}/N_0 > E_{RD}/N_0$, we have the tight approximation

$$P(e) \approx \frac{1}{\pi} \int_0^{\pi/2} \left(\frac{\sin^2\theta}{\sin^2\theta + \bar{\varepsilon_1}/2} \right)^2 d\theta \tag{C.12}$$

which gives us the closed-form expression given by (4.9) following [7].

For $E_{SD} = E_{RD}$, then $\alpha = \beta = \omega$,

$$P(e||\hat{h}_1|, |\hat{h}_2|) = Q\left(\sqrt{\frac{\rho^2\omega^2}{2\omega^2\sigma_d^2 + \sigma_n^2} (|\hat{h}_1|^2 + |\hat{h}_2|^2)} \right) \tag{C.13}$$

and $\bar{\varepsilon} = \bar{\varepsilon_1} = \bar{\varepsilon_2}$, where

$$\bar{\varepsilon} = \frac{2\omega^2 \cdot \Gamma}{2\omega^2 \cdot \nu \cdot \Gamma + 1 + \nu}. \tag{C.14}$$

Now, the BER expression is found as

$$P(e) = \frac{1}{\pi} \int_0^{\pi/2} \left(\frac{\sin^2 \theta}{\sin^2 \theta + \bar{\varepsilon}/2} \right)^2 d\theta \tag{C.15}$$

which yields (4.13) following again [7].

□ **End of chapter.**

Appendix D

Derivation of (5.68)

For general channel of ZF detector, the BER expression is in the form of $Q(\sqrt{2a})$, where

$$a = \frac{1}{N_0}\left|\rho\sqrt{E} + \sqrt{1-\rho^2}\,\frac{\alpha^2\tilde{h}_1^*\zeta_1 + \beta^2 h_2\zeta_2^*}{\sqrt{E}}\right|^2 \tag{D.1}$$

where $E = \alpha^2|\tilde{h}_1|^2 + \beta^2|h_2|^2$. Let $t_1 + jt_2$ be the fraction of the second term, for $\alpha = \beta$, it becomes,

$$a = \frac{1}{N_0}\left|\alpha\rho\sqrt{|\tilde{h}_1|^2 + |h_2|^2} + \alpha\sqrt{1-\rho^2}\cdot(t_1 + jt_2)\right|^2 \tag{D.2}$$

where $t_1 + jt_2$ represents a complex gaussian distribution and t_1 and t_2 are independent real zero-mean gaussian random variables. Then, a can be expressed in the following equation:

$$a = X_1^2 + X_2^2 = \chi^2(2) \tag{D.3}$$

where

$$X_1 = C + \sqrt{(1-\rho^2)\bar{\gamma}}\,t_1 \tag{D.4}$$

$$X_2 = \sqrt{(1-\rho^2)\bar{\gamma}}\,t_2 \tag{D.5}$$

$$C = \rho\sqrt{\left(|\tilde{h}_1|^2 + |h_2|^2\right)\bar{\gamma}} \tag{D.6}$$

$$\bar{\gamma} = \frac{\alpha^2}{N_0} \tag{D.7}$$

and $\chi^2(v)$ denotes a Chi-square distribution with v degree(s) of freedom. Given C, the distribution of a is a non-central Chi-square with 2 degrees of freedom and its probability density function is

$$P_{a|C}(a|\kappa) = \frac{\exp\left(-\frac{\kappa^2+a}{(1-\rho^2)\bar{\gamma}}\right)}{(1-\rho^2)\bar{\gamma}} J_0\left(\frac{2ja}{(1-\rho^2)\bar{\gamma}}\sqrt{a}\right) \tag{D.8}$$

where $\kappa^2 = E[X_1]^2 + E[X_2]^2$ and J_0 is a zeroth-order Bessel function of the first kind. The distribution of C is Rayleigh with 4 degrees of freedom:

$$P_C(\kappa) = \frac{2\kappa^3}{\rho^4\bar{\gamma}^2}\exp\left(-\frac{\kappa^2}{\rho^2\bar{\gamma}}\right) \tag{D.9}$$

So,

$$P_a(a) = \int_0^\infty P_{a|C}(a|\kappa)P_C(\kappa)d\kappa \tag{D.10}$$

$$= \frac{2}{\rho^4(1-\rho^2)\bar{\gamma}^3}\exp\left(-\frac{a}{(1-\rho^2)\bar{\gamma}}\right)\cdot$$
$$\int \kappa^3 \exp\left(-\frac{\kappa^2}{\rho^2(1-\rho^2)\bar{\gamma}}\right) J_0\left(\frac{2ja}{(1-\rho^2)\bar{\gamma}}\sqrt{a}\right) d\kappa. \tag{D.11}$$

Consider

$$\int_0^\infty \kappa^3 \exp\left(-\frac{\kappa^2}{\rho^2(1-\rho^2)\bar{\gamma}}\right) J_0\left(\frac{2ja}{(1-\rho^2)\bar{\gamma}}\sqrt{a}\right) d\kappa \tag{D.12}$$

$$= \frac{\rho^4(1-\rho^2)\bar{\gamma}^2\Gamma(2)}{2\Gamma(1)}\, {}_1F_1\left(2,1;\frac{\rho^2 a}{(1-\rho^2)\bar{\gamma}}\right), \tag{D.13}$$

as $\Gamma(x+1) = x\Gamma(x)$, $\Gamma(2) = \Gamma(1)$. And,

$${}_1F_1\left(2,1;\frac{\rho^2 a}{(1-\rho^2)\bar{\gamma}}\right) = \left(1+\frac{\rho^2 a}{(1-\rho^2)\bar{\gamma}}\right)\exp\left(\frac{\rho^2 a}{(1-\rho^2)\bar{\gamma}}\right). \tag{D.14}$$

Then, the distribution of a becomes

$$P_a(a) = \frac{(1-\rho^2)\bar{\gamma}+\rho^2 a}{\bar{\gamma}^2}\exp\left(-\frac{a}{\bar{\gamma}}\right). \tag{D.15}$$

Hence, by computing

$$P(e) = \int_0^\infty Q(\sqrt{2a})P_a(a)da, \tag{D.16}$$

we can obtain (5.68) in exact closed-form.

□ **End of chapter.**

Bibliography

[1] M. Abramowitz and I. A. Stegun. *Handbook of mathematical functions, with formulas, graphs, and mathematical tables.* Dover publications, INC., New York and London, 1965.

[2] S. M. Alamouti. A simple transmit diversity technique for wireless communications. *IEEE Journal on Selected Areas in Communications*, 16(8), Oct. 1998.

[3] J. K. Cavers. An analysis of pilot symbol assisted modulation for rayleigh fading channels. *IEEE Trans. Vehicular Tech.*, 40:686–693, Nov. 1991.

[4] H. T. Cheng, H. Mheidat, M. Uysal, and T. M. Lok. Distributed space-time block coding with imperfect channel estimation. In *IEEE ICC'05*, Seoul, Korea, May 2005.

[5] J. W. Craig. A new, simple and exact results for calculating the probability of error for two-dimensional signal constellations. In *IEEE MILCOM'91 Conf. Rec.*, pages 25.5.1–25.5.5, Boston, MA, US, Nov. 1991.

[6] Z. Diao, D. Shen, and V. Li. Robustness of space-time codes in the presence of channel estimation errors in ofdm systems. *IEEE PIMRC 2004*, 1:285–289, Sept. 2004.

[7] T. Eng and L. B. Milstein. Coherent ds-cdma performance in nakagami multipath fading. In *IEEE TCOM*, Feb. 1995.

[8] J. G. Foschini. Layered space-time architecture for wireless communication in a fading environment when using multi element antennas. *Bell Labs Tech. J.*, 2, Aug. 1996.

[9] I. S. Gradshteyn and I. M. Ryzhik. *Table of integrals: series and products.* Academic Press, New York and London, 1965.

[10] D. Gu and C. Leung. Performance analysis of transmit diversity scheme with imperfect channel estimation. *Electronics Letters*, 39(4):402–403, Feb. 2003.

[11] T. E. Hunter and A. Nosratinia. Performance analysis of coded cooperation diversity. *IEEE ICC'03*, 4:2688–2692, May 2003.

[12] M. Janani, A. Hedayat, T. E. Hunter, and A. Nosratinia. Coded cooperation in wireless communications: space-time transmission and iterative decoding. *IEEE Transactions on Signal Processing*, 52(2):362–371, Feb. 2004.

[13] J. N. Laneman. Network coding gain of cooperative diversity (invited paper). In *Proc. IEEE Military Comm. Conf. (MILCOM)*, Monterey, CA, Nov. 2004.

[14] J. N. Laneman and G. W. Wornell. Distributed space-time coded protocols for exploiting cooperative diversity in wireless networks. *IEEE Transactions on Information Theory*, 49(10):2415–2425, Oct. 2003.

[15] R. U. Nabar, H. Bolcskei, and F. W. Kneubuhler. Fading relay channels: performance limits and space-time signal design. *IEEE Journal on Selected Areas in Communications*, 22(6):1099–1109, Aug. 2004.

[16] A. Papoulis. *Probability, random variables and stochastic processes.* McGraw-Hill, New York, 1965.

[17] J. G. Proakis. *Digital Communications.* McGraw-Hill, Inc., 1995.

[18] J. Radon. Lineare scharen orthogonaler matrizen. *Abhandlungen aus dem Mathematischen Seminar der Hamburgishen Universitat*, 1:1–14, 1922.

[19] I. S. Reed and G. Solomon. Polynomial codes over certain finite fields. *SIAM Journal of Applied Math.*, 8:300–304, 1960.

[20] A. Ribeiro, X. Cai, and G. B. Giannakis. Opportunistic multipath for bandwidth-efficient cooperative networking. In *IEEE ICASSP' 04*, pages 549–552, May 2004.

[21] A. Ribeiro, X. Cai, and G. B. Giannakis. Symbol error probabilities for general cooperative links. In *IEEE International Conference on Communications*, pages 3369–3373, June 2004.

[22] A. Sendonaris, E. Erkip, and B. Aazhang. User cooperation diversity. part i. system description. *IEEE Transactions on Communications*, 51(11):1927–1938, Nov. 2003.

[23] A. Sendonaris, E. Erkip, and B. Aazhang. User cooperation diversity. part ii. implementation aspects and performance analysis. *IEEE Transactions on Communications*, 51(11):1939–1948, Nov. 2003.

[24] O. Shalvi. Multiple source cooperation diversity. *IEEE Communications Letters*, 8(12):712–714, Dec. 2004.

[25] W. Su and X.-G. Xia. Quasi-orthogonal space-time block codes with full diversity. pages 1098–1102, Nov. 2002.

[26] V. Tarokh, H. J. Jafarkhani, and A. R. Calderbank. Space-time block codes from orthogonal designs. *IEEE Transactions on Information Theory*, 45(5):1456–1467, July 1999.

[27] V. Tarokh, N. Seshadri, and A. R. Calderbank. Space-time codes for high data rate wireless communication: Performance criterion and code construction. *IEEE Transactions on Information Theory*, 44(2):774–765, Mar. 1998.

[28] M. Uysal and H. Mheidat. Maximum-likelihood detection for distributed space-time block coding. In *IEEE VTC'04-Fall, Los Angeles, California, USA*, Sept. 2004.

[29] A. Vielmon, Y. Li, and J. R. Barry. Performance of transmit diversity over time-varying rayleigh-fading channels. In *Proc. IEEE Global Telecommunications Conference, GLOBECOM '01*, pages 3242–3246, Nov. 2001.